

Fundamentals of Analog VLSI Design

Exercise 8 - Solution

Design of the Simple OTA

Christian Enz (christian.enz@epfl.ch)

12.11.2025

Table of contents

1	Introduction	3
2	Analysis	4
2.1	Large-signal Analysis	4
2.1.1	Voltage Transfer Characteristic	4
2.1.2	Input Common Mode Voltage Range	6
2.1.3	Slew-Rate	7
2.2	Small-signal analysis	8
2.2.1	Differential mode	8
2.2.2	Common mode	9
2.3	Noise Analysis	10
2.4	Input-referred offset voltage	13
3	Design	15
3.1	Specifications	15
3.2	Process	15
3.3	Design procedure	16
3.3.1	Sizing of M_{1a} - M_{1b}	16
3.3.2	Sizing of M_{3a} - M_{3b}	18
3.3.3	Sizing of M_{2a} - M_{2b}	18
3.4	Summary	20
3.4.1	Specifications	20
3.4.2	Bias	20
3.4.3	Transistor information	20
4	OTA Characteristics	22
4.1	Open-loop gain	22
4.2	Input-referred noise	22
4.3	Input-referred offset	23
4.4	Current and power consumption	25
5	Simulation results from ngspice	26
5.1	Operating point	26
5.2	Large-signal differential transfer characteristic	27
5.3	Open-loop gain	28
5.4	Input-referred noise	29
5.5	Input common-mode voltage range	32
5.6	Step-response	32
5.6.1	Small-step	32
5.6.2	Large step	33
5.7	Current and power consumption	34
6	Conclusion	35
	References	36

1 Introduction

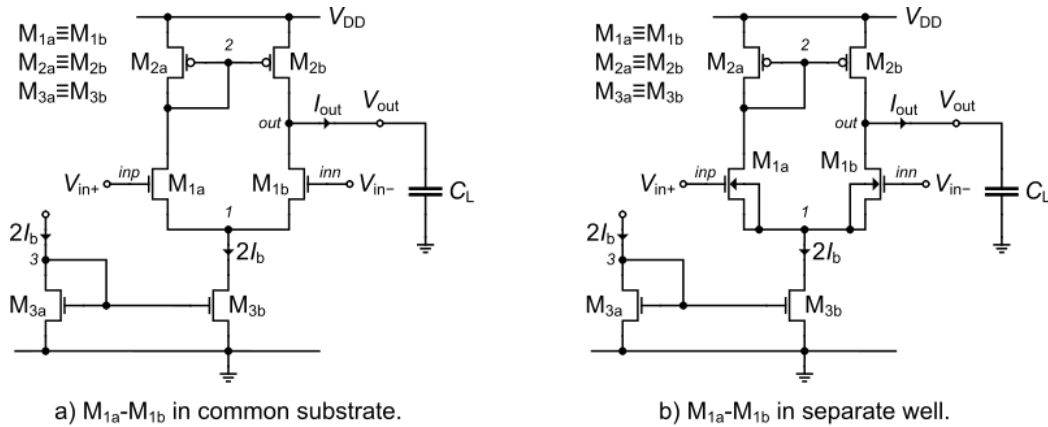


Figure 1.1: Schematic of the simple differential OTA.

Note

Note that all nMOS transistors in Figure 1.1 have an odd number and all the pMOS transistors an even number which explains the numbering process.

This notebook presents the analysis, design and simulation of the simple 5 transistors OTA presented in Figure 1.1. We can distinguish the case where M_{1a} - M_{1b} are in the common substrate (Figure 1.1 a) and the case where M_{1a} - M_{1b} are in a separate well (Figure 1.1 b). We will see below that in fully differential mode the effects of the source transconductances on the common substrate schematic are actually canceled. The design phase is using the sEKV model and the inversion coefficient approach [1], [2], [3].

The simple OTA is the simplest single-stage differential OTA having the dominant pole set by the load capacitance. We will see below that in differential mode the effects of the source transconductances on the common source node voltage are actually canceled. In order to minimize the V_{GS} voltage of M_{1a} - M_{1b} , we have chosen to put M_{1a} - M_{1b} in a separate well at the cost of a larger area.

We will start with a detailed analysis of the OTA which will allow to derive all the design equations that will be used in the design phase. The OTA is then designed for a given set of specifications for a generic 180 nm bulk CMOS technology. The design is then validated by simulations with ngspice [4] using the EKV 2.6 compact model [5] [6] [7] with parameters corresponding to a generic 180 nm bulk CMOS technology [8] [9].

We now start with the small-signal analysis.

This notebook presents the design of the simple differential OTA shown in Figure 1.1. We can distinguish the case where M_{1a} - M_{1b} are in the common substrate (Figure 1.1 a) and the case where M_{1a} - M_{1b} are in a separate well (Figure 1.1 b). We will see below that in fully differential mode the effects of the source transconductances on the common substrate schematic are actually canceled.

We will design the circuit with M_{1a} - M_{1b} in a separate well for the specifications given below. In this example, we don't give any specification on the slew-rate (SR). However the slew-rate specification can determine a bias current that is way above the one derived in this example ignoring the SR. If the SR is too high, we can move to adaptive biasing OTAs.

2 Analysis

2.1 Large-signal Analysis

2.1.1 Voltage Transfer Characteristic

Since there are two input terminals, several large-signal voltage transfer characteristics can be derived. In many situations, one of the two input terminals will be maintained at a constant common mode voltage (typically $V_{DD}/2$) while the other is connected to some feedback network. If for example the negative input is set constant, at for example the middle of the supply voltage $V_{DD}/2$, the positive input can be swept from ground to V_{DD} . The output voltage will change from ground to V_{DD} as well. The amplifier will provide some gain for V_{in+} ranging close to V_{in-} . Outside this high gain region, the output voltage will saturate either to V_{DD} for V_{in+} larger than V_{in-} , or to 0 for V_{in+} smaller than V_{in-} . Under the above conditions, the maximum output voltage $V_{out,max}$ in the linear range is limited by M_{2b} going out of saturation

$$V_{out,max} = V_{DD} - V_{SDsat2b}. \quad (2.1)$$

On the other hand, the minimum output voltage $V_{out,min}$ of the linear range is limited by M_{1b} going out of saturation and depends linearly on the common-mode voltage set on V_{in-} according to

$$V_{out,min} = V_{DSsat1b} - V_{GS1b} + V_{in-}. \quad (2.2)$$

If M_{1b} is biased in weak inversion then $V_{DSsat1b} \cong 4U_T \cong 100 \text{ mV}$. The value of V_{GS1b} depends whether M_{1a} - M_{1b} are in a separate well or are in the common substrate. The gate-to-source voltage of a transistor can be expressed from the pinch-off voltage given by

$$V_P - V_S \cong \frac{V_G - V_{T0}}{n} - V_S, \quad (2.3)$$

from which we get

$$V_G = V_{T0} + nV_S + nU_T (v_p - v_s) \quad (2.4)$$

where the normalized saturation voltage $v_p - v_s$ can be expressed in terms of the inversion coefficient as

$$v_p - v_s = \ln \left(\sqrt{4IC + 1} - 1 \right) + \sqrt{4IC + 1} - 1 - \ln(2). \quad (2.5)$$

The gate-to-source voltage is then given by

$$V_{GS} \cong V_{T0} + (n - 1) V_S + n U_T (v_p - v_s). \quad (2.6)$$

$v_p - v_s$ is equal to zero for $IC = 0.608$ and the normalized saturation voltage $v_p - v_s$ for $IC = 0.1$ is equal to -2.207 times nU_T . So in the lower part of moderate inversion and upper part of weak inversion we can approximate $v_p - v_s \cong 0$ and the gate-to-source voltage can be approximated by

$$V_{GS} \cong V_{T0} + (n - 1) V_S. \quad (2.7)$$

In case the transistor is in a separate well then $V_S = 0$, the gate-to-source voltage can simply be approximated by the threshold voltage

$$V_{GS} \cong V_{T0}. \quad (2.8)$$

In case the transistor is in the common substrate, we need to know the source voltage V_S to estimate the gate-to-source voltage according to (2.7).

2.1.1.1 M_{1a} - M_{1b} in a separate well:

In the case M_{1a} - M_{1b} are in a separate well, then $V_{S1} = 0$. If additionally, M_{1a} - M_{1b} are biased in weak inversion then $V_{DSsat1b} \cong 4U_T$ and $V_{GS1b} \cong V_{T0n}$. The minimum output voltage in the linear range is then given by

$$V_{out,min} = 4U_T - V_{T0n} + V_{in-}. \tag{2.9}$$

As long as M_{2b} remains in saturation (i.e. for $V_{out} < V_{out,max}$), the currents flowing in M_{1a} and M_{1b} are imposed equal by the current mirror. When decreasing V_{in+} and for V_{out} below $V_{out,min}$, the current in M_{1b} is equal to $I_b/2$ as long as M_{1b} remains in saturation. The gate voltage of M_{1b} is equal to V_{in-} and the source voltage of M_{1a} and M_{1b} follows V_{in+} with a shift of $V_{GS1a} \cong V_{T0n}$. Since the current is imposed equal to $I_b/2$ by the current mirror, the decrease of the source voltage increases the gate-to-source voltage of M_{1b} which has to be compensated by a decrease of the drain-to-source voltage, which is the only remaining degree of freedom in M_{1b} , to maintain the current constant at $I_b/2$. This decrease of the drain-to-source voltage of M_{1b} brings it in the linear region with a drain-to-source voltage close to zero. In such condition, the output voltage is about equal to the source voltage which decreases linearly with the positive input voltage

$$V_{out} \cong V_S = V(1) = V_{in+} - V_{GS1a} \cong V_{in+} - V_{T0n}. \tag{2.10}$$

These considerations lead to the large-signal characteristic shown in Figure 2.1 which is obtained from simulation in the case of a $0.18\text{-}\mu\text{m}$ process with $V_{DD} = 1.8\text{ V}$.

M_{1a} - M_{1b} in separate well

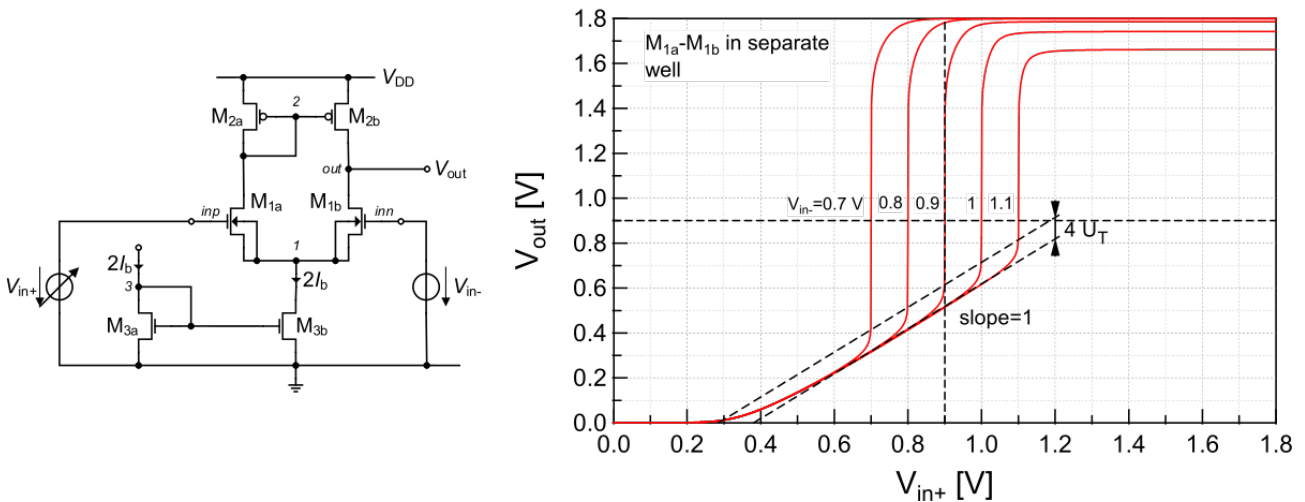


Figure 2.1: Large-signal V_{out} versus V_{in+} voltage transfer characteristic for various values of the negative input V_{in-} (M_{1a} - M_{1b} in separate well).

2.1.1.2 M_{1a} - M_{1b} in the common substrate:

In the case M_{1a} - M_{1b} are in the common substrate, the gate-to-source voltage of M_{1b} will depend on the source voltage V_S . For M_{1a} - M_{1b} biased in weak inversion we have

$$V_{GS1b} \cong V_{T0n} + (n_{1b} - 1)V_S. \tag{2.11}$$

The source voltage is also given by

$$V_S = -V_{GS1b} + V_{in-} \cong -V_{T0n} - (n_{1b} - 1)V_S + V_{in-} \tag{2.12}$$

from which we can deduce V_S as

$$V_S \cong \frac{V_{in-} - V_{T0n}}{n_{1b}} \quad (2.13)$$

The gate-to-source voltage of M_{1b} then writes

$$V_{GS1b} \cong V_{in-} - \frac{V_{in-} - V_{T0n}}{n_{1b}} \quad (2.14)$$

Finally, the minimum output voltage is given by

$$V_{out,min} \cong V_{in-} + 4U_T - V_{GS1b} = \frac{V_{in-} - V_{T0n}}{n_{1b}} + 4U_T \quad (2.15)$$

Below $V_{out,min}$, the output voltage will decrease linearly with V_{in+} with a slope $1/n_{1a}$

$$V_{out} \cong \frac{V_{in+} - V_{T0n}}{n_{1a}} \quad (2.16)$$

This is confirmed by the simulations results shown in Figure 2.2.

M_{1a} - M_{1b} in common substrate

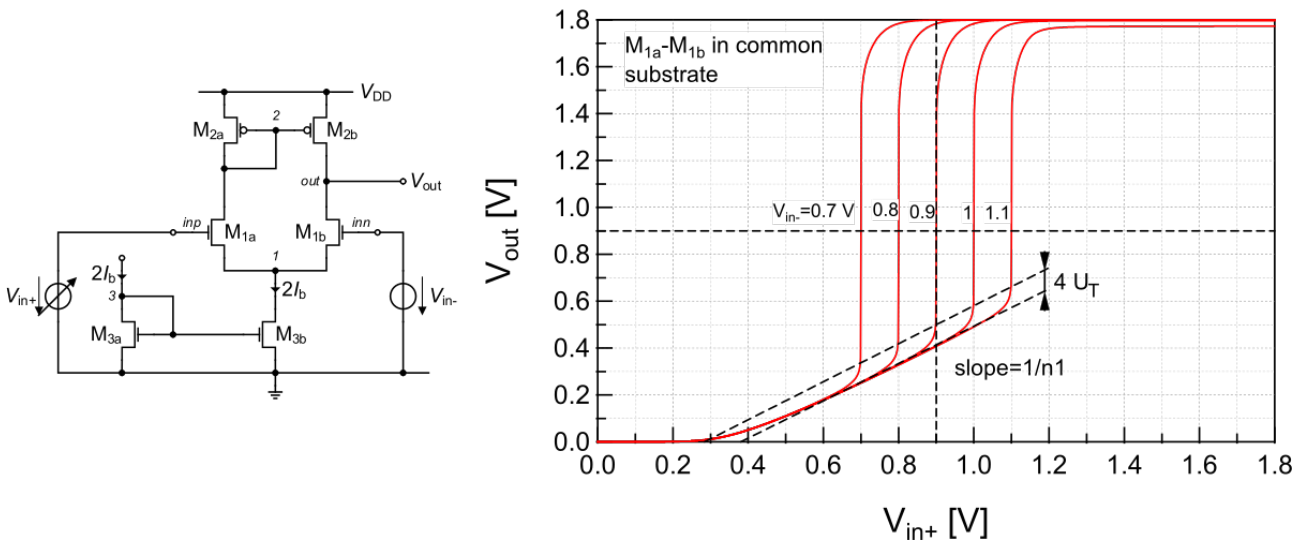


Figure 2.2: Large-signal V_{out} versus V_{in+} voltage transfer characteristic for various values of the negative input V_{in-} (M_{1a} - M_{1b} in common substrate).

2.1.2 Input Common Mode Voltage Range

The minimum common mode input voltage $V_{ic,min}$ is given by the saturation limit of M_{3b}

$$V_{ic,min} = V_{GS1} + V_{DSsat3b} \quad (2.17)$$

The maximum common mode input voltage $V_{ic,max}$ is given by the limit of saturation of M_{1a}

$$V_{ic,max} = V_{GS1a} - V_{DSsat1a} - V_{SG2} + V_{DD} \cong V_{GS1a} - 4U_T - V_{SG2} + V_{DD} \quad (2.18)$$

The gate-to-source voltage of M_{1a} V_{GS1} depends whether M_{1a} - M_{1b} are in a separate well or in the common substrate.

2.1.2.1 M_{1a} - M_{1b} in a separate well:

In the case M_{1a} - M_{1b} are biased in weak inversion and are in a separate well, $V_{GS1} \cong V_{T0n}$, and the common mode input voltage limits are given by

$$V_{ic,min} \cong V_{T0n} + V_{DSsat3b} \quad (2.19)$$

$$V_{ic,max} \cong V_{T0n} - 4U_T - V_{SG2} + V_{DD}. \quad (2.20)$$

The common mode input voltage range ΔV_{ic} is then given by

$$\Delta V_{ic} \triangleq V_{ic,max} - V_{ic,min} \cong V_{DD} - V_{SG2} - 4U_T - V_{DSsat3b}. \quad (2.21)$$

Equation (2.21) shows that although it is appropriate to bias M_{2a} - M_{2b} and M_{3a} - M_{3b} in strong inversion, choosing a too large saturation voltage will reduce the available common mode input range.

2.1.2.2 M_{1a} - M_{1b} in a common substrate:

In the case M_{1a} - M_{1b} are biased in weak inversion and are in a common substrate, the gate-to-source voltage of M_1 is given by

$$V_{GS1} \cong V_{T0n} + (n_1 - 1) \cdot V_S \quad (2.22)$$

For $V_{ic} = V_{ic,min}$, $V_S = V_{DSsat3b}$ and

$$V_{ic,min} = V_{GS1} + V_{DSsat3b} = V_{T0n} + (n_1 - 1)V_{DSsat3b} + V_{DSsat3b} = V_{T0n} + n_1 V_{DSsat3b}. \quad (2.23)$$

The source voltage for $V_{ic} = V_{ic,max}$ is equal to

$$V_S \cong V_{ic,max} - V_{GS1} = V_{ic,max} - V_{T0n} - (n_1 - 1)V_S \quad (2.24)$$

and hence

$$V_S \cong \frac{V_{ic,max} - V_{T0n}}{n_1}. \quad (2.25)$$

Replacing in (2.22) results in

$$V_{GS1} \cong V_{ic,max} - \frac{V_{ic,max} - V_{T0n}}{n_1} \quad (2.26)$$

and finally

$$V_{ic,max} \cong n_1(V_{DD} - V_{SG2} - 4U_T) + V_{T0n}. \quad (2.27)$$

Finally, the common mode input voltage range ΔV_{ic} is given by

$$\Delta V_{ic} \triangleq V_{ic,max} - V_{ic,min} \cong n_1(V_{DD} - V_{SG2} - 4U_T - V_{DSsat3b}). \quad (2.28)$$

From (2.21) and (2.28), we see that having M_{1a} - M_{1b} in the common substrate gives a common mode input voltage range n_1 larger than having them in a separate well. Since the upper limit is identical, it comes from the fact that the slope of the output voltage versus V_{in+} is $1/n_1$ which is slightly smaller than 1.

2.1.3 Slew-Rate

Assuming that the differential pair is biased in weak inversion, when the magnitude of the differential voltage becomes larger than about $4U_T$, the magnitude of the output current saturates to I_b . The OTA then behaves like a current source of value I_b loaded by the load capacitance C_L . The rate of voltage change across the load capacitance is therefore limited to a maximum given by

$$SR \triangleq \left| \frac{dV_{out}}{dt} \right|_{max} = \left| \frac{I_{out}}{C_L} \right|_{max} = \frac{I_b}{C_L}. \quad (2.29)$$

For a given load capacitance and a given available transient time, (2.29) often determines the minimum required bias current.

2.2 Small-signal analysis

The small-signal schematic corresponding to the schematics of Figure 1.1 are shown in Figure 2.3.

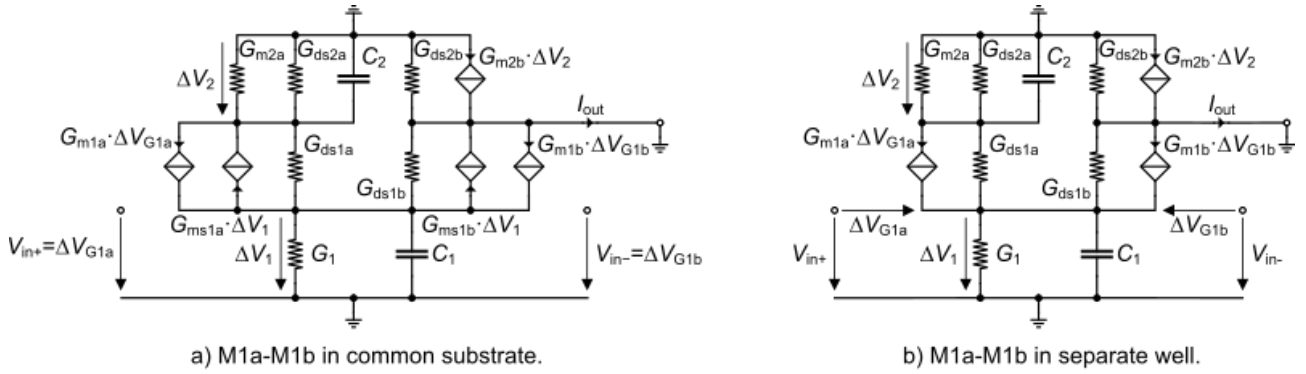


Figure 2.3: Small-signal schematic of the simple OTA.

In the case M_{1a} - M_{1b} are in the common substrate (left figure), we can recognize the source transconductances in Figure 2.3 which are controlled by the common voltage at the source ΔV_1 .

We now first look at the operation in differential mode.

2.2.1 Differential mode

In order to derive the differential transadmittance, we first will simplify the small-signal schematic of Figure 2.3 by considering that the output conductances are much smaller than the transconductances $G_{ds} \ll G_m < G_{ms}$ for all transistors. This leads to the simplified small-signal schematics shown in Figure 2.4.

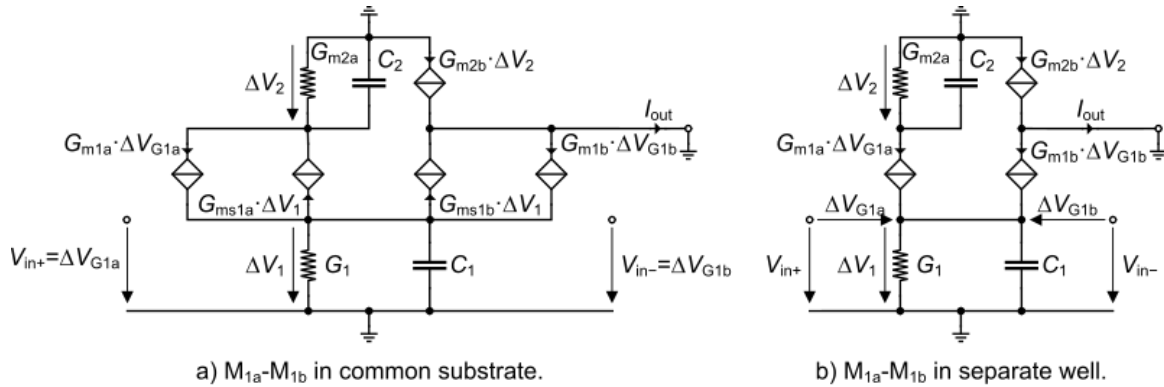


Figure 2.4: Simplified small-signal schematic.

The differential transadmittance is defined as

$$Y_{md} \triangleq \frac{I_{out}}{V_{id}}, \quad (2.30)$$

where $V_{id} \triangleq V_{in+} - V_{in-}$ is the input differential voltage and I_{out} the output current. Note that in the small-signal schematic, the output node has been connected to the ac ground. The output conductance of transistor M_{2b} G_{ds2b} is then grounded and can therefore be neglected. Also, the output conductance of transistor M_{2a} G_{ds2a} is in parallel with its transconductance G_{m2a} and since usually $G_{ds2a} \ll G_{m2a}$, it can also be neglected. Assuming a perfect matching, i.e. $G_{m1b} = G_{m1a} = G_{m1}$, $G_{ms1b} = G_{ms1a} = G_{ms1}$ and $G_{m2b} = G_{m2a} = G_{m2}$, the differential transadmittance is then given by

$$Y_{md} = G_{m1} \frac{1 + s\tau_2/2}{1 + s\tau_2} = G_{m1} \frac{1 + s/(2\omega_2)}{1 + s/\omega_2} \quad (2.31)$$

where $\tau_2 = 1/\omega_2 \triangleq C_2/G_{m2}$ is the time constant introduced by the current mirror M_{2a} - M_{2b} due to the parasitic capacitance C_2 at node 2. Note that (2.31) is valid for both M_{1a} - M_{1b} in a separate well and in a common substrate. This is due to the fact that in differential mode and assuming a perfect matching, the common source node 1 does not change and can be considered as an ac ground. This means that $\Delta V_1 = 0$ and hence the two small-signal circuits on the left and right of Figure 2.4 become identical.

The magnitude of Y_{md} normalized to the low-frequency value G_{m1} is plotted versus the frequency in Figure 2.5.

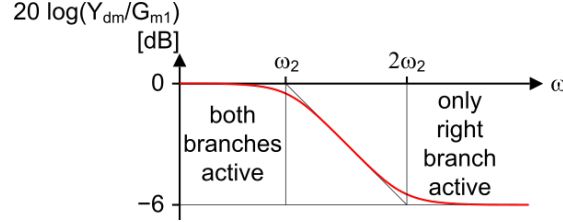


Figure 2.5: Magnitude of the transadmittance Y_{md} normalized to G_{m1} versus the frequency.

A transfer function like (2.31) is called a pole-zero doublet. This means that the zero, situated at twice the value of the pole, is canceling the effect of the pole at frequencies above the zero. For $\omega < \omega_2$, both current branches of the differential pair are active. On the other hand, for $\omega_2 < \omega$, the voltage at node 2 is low-pass filtered and ac grounded and therefore the small-signal current coming from transistor M_{1a} is not copied to the output anymore. The output current is hence only coming from transistor M_{1b} , resulting in half the low-frequency transconductance corresponding to the -6 dB asymptote shown in Figure 2.5.

The differential mode open-loop voltage transfer function A_{vd} is simply given by

$$A_{vd} \triangleq \frac{\Delta V_{out}}{V_{id}} = Y_{md} \cdot Z_L \quad (2.32)$$

where Z_L is the output load. In the case the output load is only capacitive we then have

$$Y_L \triangleq 1/Z_L = G_o + s C_L \quad (2.33)$$

where G_o is the total conductance at the output node $G_o = G_{ds1b} + G_{ds2b}$. This results in

$$A_{vd} = \frac{G_{m1}}{G_o + s C_L} \frac{1 + s/(2\omega_2)}{1 + s/\omega_2} = A_{dc} \frac{1 + s/(2\omega_2)}{(1 + s/\omega_0)(1 + s/\omega_2)} \quad (2.34)$$

where $A_{dc} \triangleq G_{m1}/G_o$ is the DC gain, $\omega_o \triangleq G_o/C_L$ the dominant pole set by the load capacitance C_L and $\omega_2 \triangleq G_{m2}/C_2$ the non-dominant due to the parasitic capacitance at the current mirror node 2. The Bode plot of the small-signal differential voltage transfer function is shown in Figure 2.6.

Assuming that the non-dominant pole ω_2 is much higher than the unity gain frequency ω_u , the latter is then given by

$$\omega_u = A_{dc} \cdot \omega_0 = \frac{G_{m1}}{G_o} \frac{G_o}{C_L} = \frac{G_{m1}}{C_L}. \quad (2.35)$$

Note that the phase reaches a minimum for $\omega = \sqrt{2}\omega_2$

$$\Phi_{min} = -\frac{\pi}{2} + \arctan(\sqrt{2}/2) - \arctan(\sqrt{2}) \cong -109.5^\circ. \quad (2.36)$$

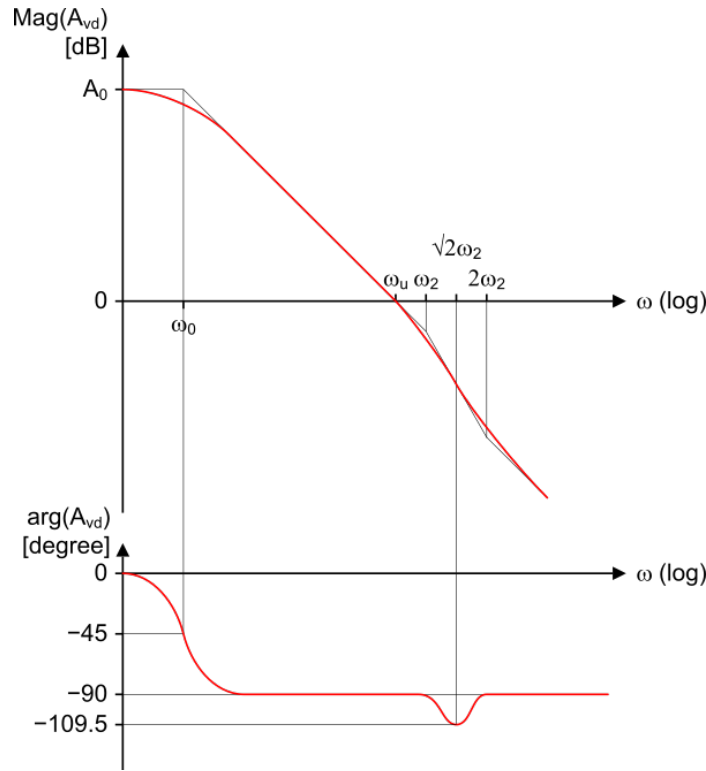


Figure 2.6: Magnitude and phase of the open-loop voltage differential gain A_{vd} normalized to G_{m1} versus the frequency.

2.2.2 Common mode

In common mode, the differential voltage is zero $V_{id} = 0$ and both inputs are controlled by the common mode voltage V_{ic} . The common mode transmittance Y_{mc} is defined as

$$Y_{mc} \triangleq \frac{I_{out}}{V_{ic}} = -G_{m1} \frac{s^2 \tau_1 \tau_2}{(1 + s\tau_1)(1 + s\tau_2)} = -G_{m1} \frac{s^2 / (\omega_1 \omega_2)}{(1 + s/\omega_1)(1 + s/\omega_2)} \quad (2.37)$$

where τ_1 corresponds to the time constant of the common source node 1 of the differential pair given by

$$\tau_1 = \frac{1}{\omega_1} = \frac{C_1}{2G_{m1}} \quad (2.38)$$

for M_{1a} - M_{1b} in a separate well and

$$\tau_1 = \frac{1}{\omega_1} = \frac{C_1}{2G_{ms1}} = \frac{C_1}{2n_1 G_{m1}} \quad (2.39)$$

for M_{1a} - M_{1b} in a common substrate. τ_2 corresponds to the time constant of the current mirror node 2 and is given by

$$\tau_2 = \frac{1}{\omega_2} \triangleq \frac{C_2}{G_{m2}}. \quad (2.40)$$

From (2.37) we see that Y_{mc} is zero at low frequency. Note that it is actually limited by the conductance at node 1 G_1 and the mismatch in the differential pair and the current mirror. At high frequency (i.e. $\omega \gg \omega_1$ and $\omega \gg \omega_2$), nodes 1 and 2 are ac grounded and the output current is directly provided by M_{1b} , so that Y_{mc} becomes equal to $-G_{m1}$.

The common-mode rejection ratio (CMMR) is then given by

$$CMRR \triangleq \frac{Y_{md}}{Y_{mc}} = -\frac{(1 + s\tau_1)(1 + s\tau_2/2)}{s^2 \tau_1 \tau_2} = -\frac{(1 + s/\omega_1)(1 + s/(2\omega_2))}{s^2 / (\omega_1 \omega_2)}, \quad (2.41)$$

which, assuming a perfect matching, is ideally infinite at low frequency and degrades for increasing frequency to reach -6dB at high frequency.

2.3 Noise Analysis

In order to calculate the noise output current I_{nout} , the input terminals are grounded. The small-signal equivalent circuit including the noise sources of all the transistors are shown in Figure 2.7.

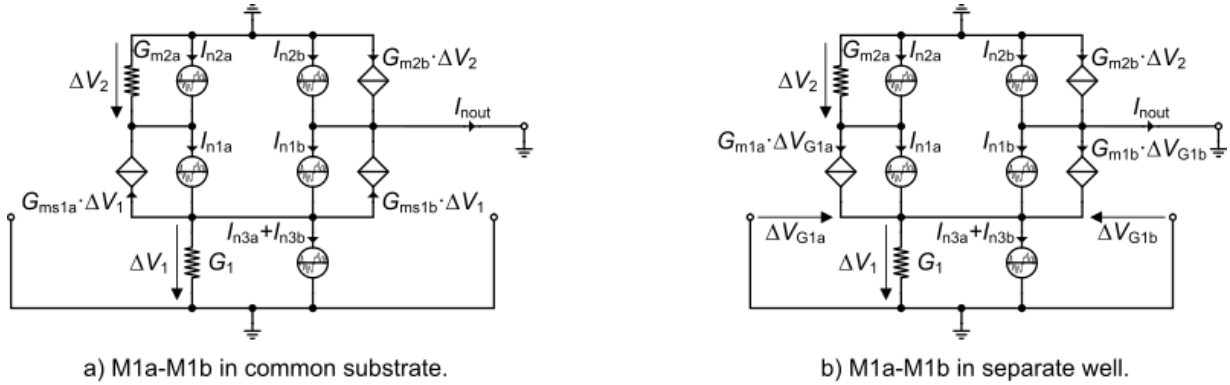


Figure 2.7: Simplified small-signal noise schematic. a) M_{1a} - M_{1b} in common substrate. b) M_{1a} - M_{1b} in separate well.

The left schematic corresponds to M_{1a} - M_{1b} in a separate well whereas the right schematic corresponds to all N-channel transistors in the same substrate. Note that all the output conductances have been neglected. Since we want to calculate the noise at low-frequency (meaning for $\omega < \omega_2$), we can neglect the parasitic capacitances C_1 and C_2 . If a perfect symmetry is assumed, then the two currents generated by transconductances G_{m1a} and G_{m1b} , or G_{ms1a} and G_{ms1b} in the above schematic are equal. If the current mirror is also assumed symmetrical, then the current coming from M_{1a} is mirrored at the output and compensated by the current coming directly from M_{1b} . Therefore, the transconductances G_{m1a} and G_{m1b} (respectively G_{ms1a} and G_{ms1b}) have no effect on the output current. They can therefore be neglected. Assuming again perfect symmetry, the noise currents I_{n3a} and I_{n3b} coming from transistors M_{3a} and M_{3b} split equally between the two branches and produce no net current at the output neither. They can therefore also be neglected. Finally, the output noise current is simply given by

$$I_{nout} = I_{n1a} - I_{n1b} - I_{n2a} + I_{n2b}. \quad (2.42)$$

This means that the transfer functions at low-frequency from each of the noise sources to the output current is simply equal to ± 1 . Note that the sign is of no importance since for noise we are only interested by the square of the magnitude of the transfer functions.

The power spectral density (PSD) of the output noise current is then given by

$$S_{nout}(f) = 4kT \cdot G_{nout}(f), \quad (2.43)$$

with

$$G_{nout}(f) = G_{n1a}(f) + G_{n1b}(f) + G_{n2a}(f) + G_{n2b}(f) = 2(G_{n1}(f) + G_{n2}(f)). \quad (2.44)$$

The noise conductances $G_{ni}(f)$ with $i = 1, 2$, are frequency dependent since they include both the thermal and the $1/f$ noise. They are given by

$$G_{ni}(f) = \gamma_{ni} \cdot G_{mi} + G_{mi}^2 \cdot \frac{\rho_i}{W_i L_i f}, \quad (2.45)$$

for $i = 1, 2$ where $\rho_1 = \rho_n$ and $\rho_2 = \rho_p$ and

$$\gamma_{ni} = \begin{cases} \frac{n_i}{2} & \text{in weak inversion} \\ \frac{2}{3} n_i & \text{in strong inversion.} \end{cases} \quad (2.46)$$

The noise can be referred to the differential input by dividing G_{nout} by G_{m1}^2 , resulting in

$$R_{nin}(f) \triangleq \frac{G_{nout}}{G_{m1}^2} = R_{nt} + R_{nf}(f) \quad (2.47)$$

where R_{nt} is the part of the input-referred noise resistance corresponding to the thermal noise

$$R_{nt} = 2 \left(\frac{\gamma_{n1}}{G_{m1}} + \gamma_{n2} \frac{G_{m2}}{G_{m1}^2} \right) = \frac{2\gamma_{n1}}{G_{m1}} \cdot (1 + \eta_{th}), \quad (2.48)$$

where

$$\eta_{th} = \frac{\gamma_{n2} G_{m2}}{\gamma_{n1} G_{m1}} \quad (2.49)$$

represents the contribution to the input-referred thermal noise of the current mirror relative to that of the differential pair.

The flicker noise resistance $R_{nf}(f)$ is the part corresponding to the 1/f noise

$$R_{nf}(f) = 2 \left[\frac{\rho_n}{W_1 L_1 f} + \left(\frac{G_{m2}}{G_{m1}} \right)^2 \frac{\rho_p}{W_2 L_2 f} \right] = \frac{2\rho_n}{W_1 L_1 f} \cdot (1 + \eta_{fl}). \quad (2.50)$$

where

$$\eta_{fl} = \left(\frac{G_{m2}}{G_{m1}} \right)^2 \frac{\rho_p W_1 L_1}{\rho_n W_2 L_2} \quad (2.51)$$

represents the contribution to the input-referred flicker noise of the current mirror relative to the differential pair.

In the same way a noise excess factor γ_n has been defined for a single transistor, a thermal noise excess factor can also be defined for the complete OTA as

$$\gamma_{ota} \triangleq G_m \cdot R_{nt} = \frac{G_{nout,thermal}}{G_m} = 2\gamma_{n1} \cdot (1 + \eta_{th}) \quad (2.52)$$

where $G_m = G_{m1}$ is the OTA differential transconductance. The total input-referred thermal noise resistance then writes

$$R_{nt} = \frac{\gamma_{ota}}{G_{m1}}. \quad (2.53)$$

The minimum value of the OTA noise excess factor is equal to that of the differential pair only, namely $\gamma_{ota,min} = 2\gamma_{n1}$. In order to limit the contribution of the current mirror to a minimum, the second term in the bracket of (2.52) should be made much smaller than one. This can be achieved by setting the transconductance ratio $G_{m2}/G_{m1} \ll 1$. This can be done by biasing M_{1a}-M_{1b} in weak inversion and M₂-M_{2b} in strong inversion, respectively. Replacing G_{m2}/G_{m1} by

$$\frac{G_{m2}}{G_{m1}} = \frac{2n_1 U_T}{n_2 V_{DSsat2}} = \frac{2n_1 U_T}{n_2 V_{P2}} \cong \frac{2n_1 U_T}{V_{G2} - V_{TOp}} \quad (2.54)$$

results in

$$\gamma_{ota} = 2\gamma_{n1} \left(1 + \frac{\gamma_{n2}}{\gamma_{n1}} \frac{2n_1 U_T}{V_{G2} - V_{TOp}} \right) = n_1 \left(1 + \frac{8n_2}{3} \frac{U_T}{V_{G2} - V_{TOp}} \right), \quad (2.55)$$

where $\gamma_{n1} = n_1/2$ and $\gamma_{n2} = n_2/3$. The OTA thermal noise excess factor is therefore minimized by setting the transconductance ratio $G_{m2}/G_{m1} \ll 1$, which is realized easily if transistors M_{1a}-M_{1b} are biased in weak inversion and M₂-M_{2b} in strong inversion and by choosing an overdrive voltage $V_{G2} - V_{TOp}$ of M₂-M_{2b} much larger than $8n_2/3U_T \cong 4U_T$ where it has been assumed that $n_2 \cong 3/2$.

The 1/f noise corner frequency f_k is defined as the frequency at which the 1/f noise becomes equal to the thermal noise

$$R_{nf}(f_k) = R_{nt} \quad (2.56)$$

and is given by

$$f_k = \frac{G_{m1}}{\gamma_{ota}} \frac{2\rho_n}{W_1 L_1} \cdot (1 + \eta_{fl}). \quad (2.57)$$

The corner frequency can be reduced by increasing $W_1 L_1$ and $W_2 L_2$ at the same time to conserve the same η_{fl} factor. Of course increasing the area of transistors M₁ and M₂ increases the parasitic capacitance at node 2 and hence decreases the non-dominant pole ω_2 .

2.4 Input-referred offset voltage

Mismatch between the two transistors of the differential pair M_{1a} - M_{1b} and of the current mirror M_{2a} - M_{2b} causes some current to flow at the output even for a zero differential input voltage $V_{id} = 0$. This output current can be compensated by applying a certain differential input voltage defined as the input-referred offset voltage V_{os} .

The analysis of the mismatch effects for deriving the variance of the input-referred offset voltage can be done similarly to the noise analysis. We can reuse (2.42) with

$$I_{n1a} = +\frac{\Delta I_{D1}}{2}, \quad (2.58)$$

$$I_{n1b} = -\frac{\Delta I_{D1}}{2}, \quad (2.59)$$

$$I_{n2a} = -\frac{\Delta I_{D2}}{2}, \quad (2.60)$$

$$I_{n2b} = +\frac{\Delta I_{D2}}{2}, \quad (2.61)$$

and where ΔI_{D1} and ΔI_{D2} are the current mismatch in the differential pair and in the current mirror, respectively. The output current due to these current mismatches is then given by

$$I_{out} = \Delta I_{D1} + \Delta I_{D2}. \quad (2.62)$$

Of course ΔI_{D1} and ΔI_{D2} are random variables. The variance of the offset output current is then given by

$$\sigma_{I_{out}}^2 = \sigma_{\Delta I_{D1}}^2 + \sigma_{\Delta I_{D2}}^2 = I_b^2 \cdot \left(\sigma_{\Delta I_{D1}/I_{D1}}^2 + \sigma_{\Delta I_{D2}/I_{D2}}^2 \right) \quad (2.63)$$

where

$$\sigma_{\Delta I_{D1}/I_{D1}}^2 = \sigma_{\beta 1}^2 + \left(\frac{G_{m1}}{I_b} \right)^2 \sigma_{VT1}^2, \quad (2.64)$$

$$\sigma_{\Delta I_{D2}/I_{D2}}^2 = \sigma_{\beta 2}^2 + \left(\frac{G_{m2}}{I_b} \right)^2 \sigma_{VT2}^2. \quad (2.65)$$

with

$$\sigma_{\beta i}^2 = \frac{A_\beta^2}{W_i L_i}, \quad (2.66)$$

$$\sigma_{VT0i}^2 = \frac{A_{VT}^2}{W_i L_i}. \quad (2.67)$$

for $i = 1, 2$. A_β (usually given in $\% \cdot \mu\text{m}$) and A_{VT} (usually given in $\text{mV} \cdot \mu\text{m}$) are the β and threshold matching parameters for the process to be used.

The variance of the output offset current then writes

$$\sigma_{I_{out}}^2 = I_b^2 \cdot \left(\sigma_{\beta 1}^2 + \sigma_{\beta 2}^2 \right) + G_{m1}^2 \sigma_{VT1}^2 + G_{m2}^2 \sigma_{VT2}^2. \quad (2.68)$$

The variance of the input-referred offset voltage is obtained by dividing the variance of the output offset current (2.68) by G_{m1}^2 resulting in

$$\sigma_{V_{os}}^2 = \left(\frac{I_b}{G_{m1}} \right)^2 \left(\sigma_{\beta 1}^2 + \sigma_{\beta 2}^2 \right) + \left(\frac{G_{m2}}{G_{m1}} \right)^2 \sigma_{VT2}^2 + \sigma_{VT1}^2. \quad (2.69)$$

which can be written as

$$\sigma_{V_{os}}^2 = \sigma_{VT}^2 + \sigma_\beta^2, \quad (2.70)$$

where σ_{VT} is the V_T -mismatch given by

$$\sigma_{VT}^2 = \sigma_{VT1}^2 \cdot (1 + \xi_{VT}). \quad (2.71)$$

where ξ_{VT} represents the V_T -mismatch contribution to the input-referred offset of the current mirror relative to that of the differential pair

$$\xi_{VT} = \left(\frac{G_{m2}}{G_{m1}}\right)^2 \cdot \frac{\sigma_{VT2}^2}{\sigma_{VT1}^2} = \left(\frac{G_{m2}}{G_{m1}}\right)^2 \cdot \left(\frac{A_{VTp}}{A_{VTn}}\right)^2 \cdot \frac{W_1 L_1}{W_2 L_2}. \quad (2.72)$$

σ_β is the β -mismatch given by

$$\sigma_\beta^2 = \left(\frac{I_b}{G_{m1}}\right)^2 \cdot \sigma_{\beta_1}^2 \cdot (1 + \xi_\beta), \quad (2.73)$$

where ξ_β represents the β -mismatch contributions to the input-referred offset of the current mirror relative to that of the differential pair

$$\xi_\beta = \frac{\sigma_{\beta_2}^2}{\sigma_{\beta_1}^2} = \left(\frac{A_{\beta p}}{A_{\beta n}}\right)^2 \cdot \frac{W_1 L_1}{W_2 L_2}. \quad (2.74)$$

From (2.73), we see that the contribution of the β mismatch to the input-referred offset voltage can be minimized by choosing I_b/G_{m1} as small as possible (or G_{m1}/I_b as large as possible). This can be done by biasing the transistors of the differential pair in weak inversion. Secondly, from (2.72) we see that the contribution of the V_T mismatch of the current mirror ξ_{VT} can also be minimized by setting $G_{m2}/G_{m1} \ll 1$. Since M_{1a} and M_{2a} (M_{1b} and M_{2b}) share the same bias current $I_{D1} = I_{D2} = I_b$, this can only be done by biasing the current mirror M_{2a} - M_{2b} in strong inversion. In this case, the transconductances of M_1 and M_2 are then given by $G_{m1} = I_b/(n_1 U_T)$ and $G_{m2} = 2I_b/(n_2 V_{DSsat2})$ with $V_{DSsat} = V_{P2}$, leading to

$$\frac{G_{m2}}{G_{m1}} = \frac{2n_1 U_T}{n_2 V_{DSsat2}} = \frac{2n_1 U_T}{n_2 V_{P2}} \cong \frac{2n_1 U_T}{V_{G2} - V_{TOp}} \quad (2.75)$$

The overdrive voltage of M_{2a} - M_{2b} $V_{G2} - V_{TOp}$ has therefore to be chosen much larger than $2n_1 U_T$. However, the overdrive voltage $V_{G2} - V_{TOp}$ cannot be made too large since it will lead to a large V_{SG2} voltage that, for a given input common mode voltage, will push M_{1a} out of saturation.

3 Design

3.1 Specifications

The OTA specifications are given in Table 3.1.

i Note

The specifications given in Table 3.1 are simplified specifications. They are mainly targeting the achievement of a certain gain-bandwidth product GBW and DC gain at lowest current consumption. The GBW sets the differential pair transconductance while the DC gain sets the output conductance. There is an additional specification on the random input-referred offset voltage which, if not met, might eventually require to increase the transistors area. There are no specifications on thermal noise since the transconductance is set by the GBW . There are no specifications on the flicker noise but if the corner frequency was set lower this would required to increase the transistors area. There are also no specifications on the slew-rate, which might be small because of the low-power objective. Finally, there are many more specifications such as CMRR, PSRR, input common-mode voltage range, output-voltage swing, etc. . . that are not discussed in this example.

Table 3.1: OTA specifications.

Specification	Symbol	Value	Unit
Minimum DC gain	A_{dc}	60	dB
Minimum gain-bandwidth product	GBW	10	MHz
Load capacitance	C_L	0.1	pF
Maximum input-referred offset voltage	$V_{os,max}$	4	mV

3.2 Process

We will design the simple OTA for a generic 180nm bulk CMOS process. The physical parameters are given in Table 3.2, the global process parameters in Table 3.3 and finally the MOSFET parameters in Table 3.4.

Table 3.2: Physical parameters

Parameter	Value	Unit
T	300	K
U_T	25.875	mV

Table 3.3: Global process parameters

Parameter	Value	Unit
V_{DD}	1.8	V
C_{ox}	8.443	$\frac{fF}{\mu m^2}$
W_{min}	200	nm
L_{min}	180	nm

Table 3.4: Transistor process parameters

Parameter	NMOS	PMOS	Unit
sEKV parameters			
n	1.27	1.31	-
$I_{spec\Box}$	715	173	nA
V_{T0}	0.455	0.445	V
L_{sat}	26	36	nm
λ	20	20	$\frac{V}{\mu m}$
Overlap capacitances parameters			
C_{GDo}	0.366	0.329	$\frac{fF}{\mu m}$
C_{GSo}	0.366	0.329	$\frac{fF}{\mu m}$
C_{GBo}	0	0	$\frac{fF}{\mu m}$
Junction capacitances parameters			
C_J	1	1.121	$\frac{fF}{\mu m^2}$
C_{JSW}	0.2	0.248	$\frac{fF}{\mu m}$
Flicker noise parameters			
K_F	8.1e-24	6.8e-23	J
AF	1	1	-
ρ	0.05794	0.4828	$\frac{V \cdot m^2}{A \cdot s}$
Matching parameters			
A_{VT}	5	5	mV · μm
A_β	1	1	% · μm
Source and drain sheet resistance parameter			
R_{sh}	600	2386	$\frac{\Omega}{\mu m}$
Width and length parameters			
ΔW	39	54	nm
ΔL	-76	-72	nm

3.3 Design procedure

! Important

For this process, the transistor dimensions are rounded to 10nm. We also will ignore the length and width reduction parameters DL and DW . The main reason is that most of the transistor length and width are sufficiently large that ignoring these parameters has little impact.

3.3.1 Sizing of M_{1a} - M_{1b}

M_{1a} - M_{1b} are biased in weak inversion in order to

- maximize the G_m/I_D ratio and
- minimize the input-referred offset.

They are sized according to the specification on the GBW and the load capacitance and the required slew-rate. Recalling that

$$GBW = \frac{G_{m1}}{2\pi C_{out}}, \quad (3.1)$$

where G_{m1} is the gate transconductance of M_{1a} - M_{1b} and C_{out} is the total output capacitance which includes the parasitic capacitance and the load capacitance C_L . Since we do not yet know the sizes of M_{1a} and M_{2b} , we cannot estimate the total output capacitance. We will start assuming $C_{out} = C_L$. G_{m1} is then set by the GBW as

$$G_{m1} \cong 2\pi GBW C_L. \quad (3.2)$$

This gives a required transconductance $G_{m1} = 6.283 \mu A/V$. The minimum current to achieve this transconductance is obtained in weak inversion where G_{m1} is given by

$$G_{m1} = \frac{I_b}{nU_T}, \quad (3.3)$$

resulting in a minimum bias current given by

$$I_{b,min} = 2\pi n_0n U_T C_L GBW. \quad (3.4)$$

For the given specifications we get $I_{b,min} = 207 nA$. In order to achieve the high gain-bandwidth product, we have to be particularly careful about the parasitic capacitances at the output and current mirror. Setting the inversion coefficient of M_{1a} - M_{1b} too low will lead to a large transistor and hence a large capacitance at the drain of M_{1b} which adds to the load capacitance. We will choose to bias M_{1a} - M_{1b} in moderate inversion with $IC_1 = 1.0$. This gives a normalized $G_m n U_T/I_D = 0.618$ and $I_b = 334 nA$.

The corresponding slew-rate is then equal to $SR_{min} = 3.344 V/\mu s$ which we will consider as sufficient.

! Important

If the slew-rate is not sufficient, the bias current I_b should be increased resulting in a higher current and power consumption. Other options include the use of a class AB OTA [10] or a dynamic/adaptive biasing OTA [11].

To have some margin to account for the additional parasitic capacitance at the output due to the junction capacitances that add to the load capacitance C_L , we set $I_b = 350 nA$ and the inversion coefficient to $IC_1 = 1.0$. The transconductance can be calculated from the G_m/I_D function as $G_{m1} = 6.576 \mu A/V$. This leads to a gain-bandwidth product $GBW = 10.5 MHz$, which is slightly higher than the target specification offering some margin.

Knowing the drain current I_{D1} and the inversion coefficient, we can calculate the W/L aspect ratio for M_{1a} - M_{1b} as $W_1/L_1 = 0.490$. The degree of freedom left (W_1 or L_1) can be determined by constraints either on the DC gain, the offset voltage or the flicker noise. In this example we will set a minimum DC gain. The latter is given by

$$A_{dc} = \frac{G_{m1}}{G_o} \quad (3.5)$$

where $G_o = G_{ds1b} + G_{ds2b}$ is the small-signal conductance to the AC ground at the output node. The output conductances are estimated with the following simple model

$$G_{dsi} = \frac{I_{Di}}{V_{Mi}} \quad (3.6)$$

with $V_{Mi} = \lambda_i \cdot L_i$. Note that this model of the output conductance is only a very rough approximation and the gain should therefore be checked by simulation. Some margin can be taken to ensure a sufficient DC gain.

A good trade-off for the output conductance is to split the output conductance G_o equally between M_{1b} and M_{2b} $G_{ds1b} = G_{ds2b} = G_o/2$ or since M_{1a} - M_{2b} share the same bias current $V_{M1b} = V_{M2b}$. The minimum length of M_{1a} - M_{1b} is then given by $L_1 = 5.32 \mu m$, which gives a width $W_1 = 2.60 \mu m$.

3.3.2 Sizing of M_{3a} - M_{3b}

The sizing of M_{3a} - M_{3b} is conditioned by the minimum common-mode input voltage $V_{ic,min}$ to be handled according to

$$V_{ic,min} = V_{GS1} + V_{DSsat3}. \quad (3.7)$$

Because long-channel nMOS transistors have a small threshold voltage in this technology, the minimum common-mode input voltage $V_{ic,min}$ can be low. If we choose an inversion coefficient for M_{3a} - M_{3b} equal to $IC_3 = 20$, we get $V_{DSsat3} = 254 mV$ and $V_{ic,min} = 733 mV$, which is low enough. We then get the specific current $I_{spec3} = 14.300 \mu A$ and aspect ratio $W_3/L_3 = 0.049$. Since this W/L is rather small, we need to set $W_3 = W_{min} = 200 nm$, and calculate the length $L_3 = 4.09 \mu m$.

We can now size the current mirror M_{2a} - M_{2b} .

3.3.3 Sizing of M_{2a} - M_{2b}

The gate voltage of M_{2a} should be set as low as possible for a given maximum common mode input voltage still keeping M_{1a} in saturation. For a maximum input common-mode voltage $V_{ic,max}$, the source-to-gate voltage of M_{2a} V_{SG2a} is given by

$$V_{SG2a} = V_{DD} - V_{ic,max} + V_{GS1a} - V_{DSsat1a}. \quad (3.8)$$

The saturation voltage of M_{1a} - M_{1b} only depends on IC_1 . For the chosen $IC_1 = 1.0$ it is given by $V_{DSsat1a} = 116 mV$.

The gate-to-source voltage V_{GS1a} is given by

$$V_{GS1a} = V_{T0n} + (n_{0n} - 1)V_{S1} + n_{0n}U_T(v_p - v_s). \quad (3.9)$$

In this design we have chosen to put M_{1a} - M_{1b} in a separate well, hence $V_{SB1} = 0$ and V_{GS1a} reduces to

$$V_{GS1a} = V_{T0n} + n_{0n}U_T(v_p - v_s), \quad (3.10)$$

where $v_p - v_s$ can be estimated from the inversion coefficient IC_1 . For the chosen $IC_1 = 1.0$, this gives $V_{GS1} \cong 480 mV$. Setting the maximum input common-mode voltage to $V_{ic,max} = 1.3 V$, results in $V_{SG2} = 864 mV$, which corresponds to an inversion coefficient $IC_2 = 34.1$.

Because V_{SG2} also sets the quiescent output voltage, we could slightly increase V_{SG2} so that the quiescent output voltage is set at $V_{DD}/2 = 0.9 V$. Choosing $V_{SG2} = 900 mV$, corresponds to an inversion coefficient $IC_2 = 40.1$ and a saturation voltage $V_{DSsat2} = 343 mV$. The specific current is then $I_{spec2} = 8.74 nA$, the aspect ratio $W_2/L_2 = 0.050$ and the transconductance $G_{m2} = 1.512 \mu A/V$,

The length of M_{2a} - M_{2b} is set by the dc gain similarly to the length of M_{1a} - M_{1b} resulting in $L_2 = 5.32 \mu m$ from which we get its width $W_2 = 270 nm$.

Since G_{m2} may become small and the gate area of M_{2a} - M_{2b} large, we need to check whether the non-dominant pole f_{p2} lies sufficiently high above the GBW to insure the desired phase margin. The non-dominant pole is given by

$$\omega_{p2} = \frac{G_{m2}}{C_2}, \quad (3.11)$$

where C_2 is given by

$$C_2 = 2(C_{GS2} + C_{GB2}) \quad (3.12)$$

Assuming M_2 is in saturation, we have

$$C_{GS2} \cong W_2 L_2 C_{ox} \cdot c_{gsi} + C_{GSop} \cdot W_2 \quad (3.13)$$

where c_{gsi} is the normalized intrinsic gate-to-source capacitance which is typically equal to $2/3$ in strong inversion and is proportionnal to IC in weak inversion. The gate-to-bulk capacitance C_{GB2} is given by

$$C_{GB2} \cong W_2 L_2 C_{ox} \cdot c_{gbi} + C_{GBop} \cdot W_2, \quad (3.14)$$

where c_{gbi} is the normalized gate-to-bulk intrinsic capacitance given by

$$c_{gbi} = \frac{n-1}{n} \cdot c_{gsi}. \quad (3.15)$$

The capacitance at node 2 scales with W_2 and L_2 according to

$$C_2 = C_{WL} \cdot W_2 L_2 + C_W \cdot W_2, \quad (3.16)$$

with

$$C_{WL} = 2 C_{ox} \cdot (c_{gsi} + c_{gbi}), \quad (3.17)$$

$$C_W = 2(C_{GSop} + C_{GBop}). \quad (3.18)$$

For the W_2 and L_2 chosen above, this results in $C_{GS2} = 7.50 \text{ fF}$, $C_{GB2} = 1.11 \text{ fF}$, $C_2 = 17.21 \text{ fF}$ and finally $f_{p2} = 13.988 \text{ MHz}$, which is close to the specified GBW .

We therefore need to reduce IC_2 which will increase the G_m/I_D and since the current is set by the bias current I_b , it will increase G_{m2} . If W_2 is set to its minimum value W_{min} , decreasing IC_2 keeping the same current, will increase the W_2/L_2 . With W_2 set, this leads to a decrease of L_2 and hence a decrease of C_2 . The increase of G_{m2} and decrease of C_2 leads to an increase of f_{p2} , as required. We can use the following script to find the required IC for having the non-dominant pole at 10 times the GBW .

Running the optimizer results in an inversion coefficient $IC_2 = 14.7$, a transconductance $G_{m2} = 2.375 \mu A/V$, a transconductance ratio $G_{m1}/G_{m2} = 2.769$, an aspect ratio $W_2/L_2 = 0.138$ and finally a width and length $W_2 = 200 \text{ nm}$ and $L_2 = 1.45 \mu m$. As expected, the non-dominant pole is $f_{p2} = 100 \text{ MHz}$ corresponding to the target ratio $f_{p2}/GBW = 10$.

We see that IC_2 has been increased, increasing G_{m2} and W_2/L_2 for the given current I_b . Since W_2 hits W_{min} , the length L_2 has been slightly increased, increasing C_2 at the same time to set f_{p2} at 10 times the GBW . Now, this has also increased V_{SG2}

$$V_{SG2} = 713 \text{ mV},$$

which reduces the maximum input common-mode voltage to

$$V_{ic,max} = 1.451 \text{ V}.$$

The sizing process is now finished. The resulting design is summarized in the next section.

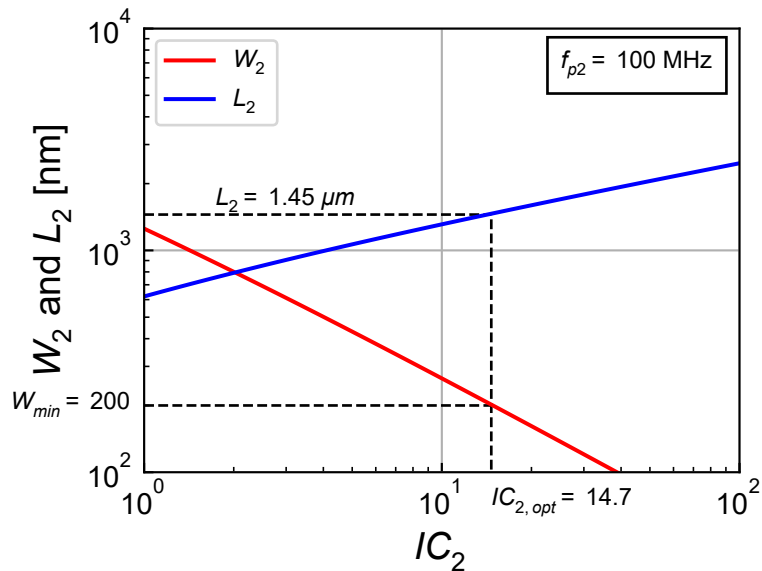


Figure 3.1: Length L_2 and width W_2 of M_{2a} - M_{2b} versus IC_2 for a given f_{p2}/GBW ratio.

3.4 Summary

3.4.1 Specifications

The specifications are recalled in Table 3.5.

Table 3.5: OTA specifications.

Specification	Symbol	Value	Unit
Minimum DC gain	A_{dc}	60	dB
Minimum gain-bandwidth product	GBW	10	MHz
Load capacitance	C_L	0.1	pF
Maximum input-referred random offset voltage	$V_{os,max}$	4	mV
Phase margin	PM	60	$^\circ$

3.4.2 Bias

The bias information are summarized in Table 3.6.

Table 3.6: OTA bias.

Bias voltage or current	Symbol	Value	Unit
Supply voltage	V_{DD}	1.8	V
Bias current	I_b	350	nA

3.4.3 Transistor information

The transistor sizes and large-signal variables are summarized in Table 3.7, whereas Table 3.8 gives the small-signal and thermal noise parameters. An Excel table is generated with more information (e.g. all the parasitic capacitances).

Table 3.7: Transistor size and bias information.

Transistor	W [μm]	L [μm]	I_D [nA]	I_{spec} [nA]	IC	$V_G - V_{T0}$ [mV]	V_{DSsat} [mV]
M1a	2.60	5.32	350	349	1.0	15	116
M1b	2.60	5.32	350	349	1.0	15	116
M2a	0.20	1.45	350	24	14.7	157	224
M2b	0.20	1.45	350	24	14.7	157	224
M3a	0.20	4.09	700	35	20.0	191	254
M3b	0.20	4.09	700	35	20.0	191	254

Table 3.8: Transistor small-signal and thermal noise parameters.

Transistor	G_{spec} [$\mu A/V$]	G_{ms} [$\mu A/V$]	G_m [$\mu A/V$]	G_{ds} [nA/V]	γ_n
M1a	13.505	8.356	6.573	3.289	0.717
M1b	13.505	8.356	6.573	3.289	0.717
M2a	0.923	3.101	2.375	12.066	0.821
M2b	0.923	3.101	2.375	12.066	0.821
M3a	1.351	5.408	4.254	8.557	0.805
M3b	1.351	5.408	4.254	8.557	0.805

4 OTA Characteristics

In this section, we check whether the specs are achieved.

4.1 Open-loop gain

The calculated OTA features are given in Table 4.1.

Table 4.1: OTA gain variables.

Symbol	Theoretical Value	Unit
A_{dc}	53	dB
G_{m1}	6.573	$\mu A/V$
G_{m2}	2.375	$\mu A/V$
f_0	24.438	kHz
GBW	10.461	MHz
f_{p2}	110.282	MHz
f_{z2}	220.563	MHz

⚠ Warning

The slight differences between the value of f_{p2} calculated during the design process and the value shown in Table 4.1 is due to the width and length rounding process.

Using the values given in Table 4.1, we can now plot the gain response shown in Figure 4.1.

4.2 Input-referred noise

We can now compute all the parameters needed for the calculation of the OTA thermal noise excess factor and its input-referred thermal noise resistance. They are given in Table 4.2.

Table 4.2: OTA thermal noise parameters.

Symbol	Theoretical Value	Unit
G_{m1}	6.573	$\mu A/V$
G_{m2}	2.375	$\mu A/V$
G_{m1}/G_{m2}	2.768	-
γ_{n1}	0.717	-
γ_{n2}	0.821	-
η_{th}	0.414	-
R_{nt}	308.316	$k\Omega$
γ_{ota}	2.026	-
$\sqrt{S_{ninth}}$	71.454	nV/\sqrt{Hz}
$10 \cdot \log(S_{ninth})$	-142.919	dBv/\sqrt{Hz}

Table 4.2: OTA thermal noise parameters.

Symbol	Theoretical Value	Unit
--------	-------------------	------

From Table 4.2, we see that $\eta_{th} = 0.414$ and hence that the OTA thermal noise excess factor is only slightly larger than that of the differential pair. This is due to the G_{m1}/G_{m2} ratio as shown in Table 4.2.

We can now compute all the parameters needed for the calculation of the input-referred flicker noise and the corner frequency. They are given in Table 4.3.

Table 4.3: OTA flicker noise parameters.

Symbol	Theoretical Value	Unit
$(G_{m1}/G_{m2})^2$	7.7	-
ρ_p/ρ_n	8.3	-
$\frac{W_1 \cdot L_1}{W_2 \cdot L_2}$	47.7	-
η_{fl}	42.997	-
$\sqrt{S_{ninf1}(1 Hz)}$	78.1	$\mu V/\sqrt{Hz}$
$10 \cdot \log(S_{ninf1}(1 Hz))$	-82.1	dBv/\sqrt{Hz}
f_k	1195	kHz

From Table 4.3, we see that M_{2a} - M_{2b} contribute 42.997 times more than M_{1a} - M_{1b} . This is coming from the fact that $W_1 L_1$ is 48 times larger than $W_2 L_2$ and that ρ_p is 8.3 times larger than ρ_n . The flicker noise will therefore be dominated by M_{2a} - M_{2b} .

We can plot the input-referred noise which is shown in Figure 4.2.

4.3 Input-referred offset

The variance of the input-referred offset is given by (2.70) which is repeated below

$$\sigma_{V_{os}}^2 = \sigma_{V_T}^2 + \sigma_{\beta}^2, \quad (4.1)$$

where σ_{V_T} is the V_T -mismatch given by

$$\sigma_{V_T}^2 = \sigma_{V_{T1}}^2 \cdot (1 + \xi_{V_T}). \quad (4.2)$$

where ξ_{V_T} represents the V_T -mismatch contribution to the input-referred offset of the current mirror relative to that of the differential pair

$$\xi_{V_T} = \left(\frac{G_{m2}}{G_{m1}} \right)^2 \cdot \frac{\sigma_{V_{T2}}^2}{\sigma_{V_{T1}}^2} = \left(\frac{G_{m2}}{G_{m1}} \right)^2 \cdot \left(\frac{A_{V_{Tp}}}{A_{V_{Tp}}} \right)^2 \cdot \frac{W_1 L_1}{W_2 L_2}. \quad (4.3)$$

σ_{β} is the β -mismatch given by

$$\sigma_{\beta}^2 = \left(\frac{I_b}{G_{m1}} \right)^2 \cdot \sigma_{\beta_1}^2 \cdot (1 + \xi_{\beta}), \quad (4.4)$$

where ξ_{β} represents the β -mismatch contributions to the input-referred offset of the current mirror relative to that of the differential pair

$$\xi_{\beta} = \frac{\sigma_{\beta_2}^2}{\sigma_{\beta_1}^2} = \left(\frac{A_{\beta_p}}{A_{\beta_n}} \right)^2 \cdot \frac{W_1 L_1}{W_2 L_2}, \quad (4.5)$$

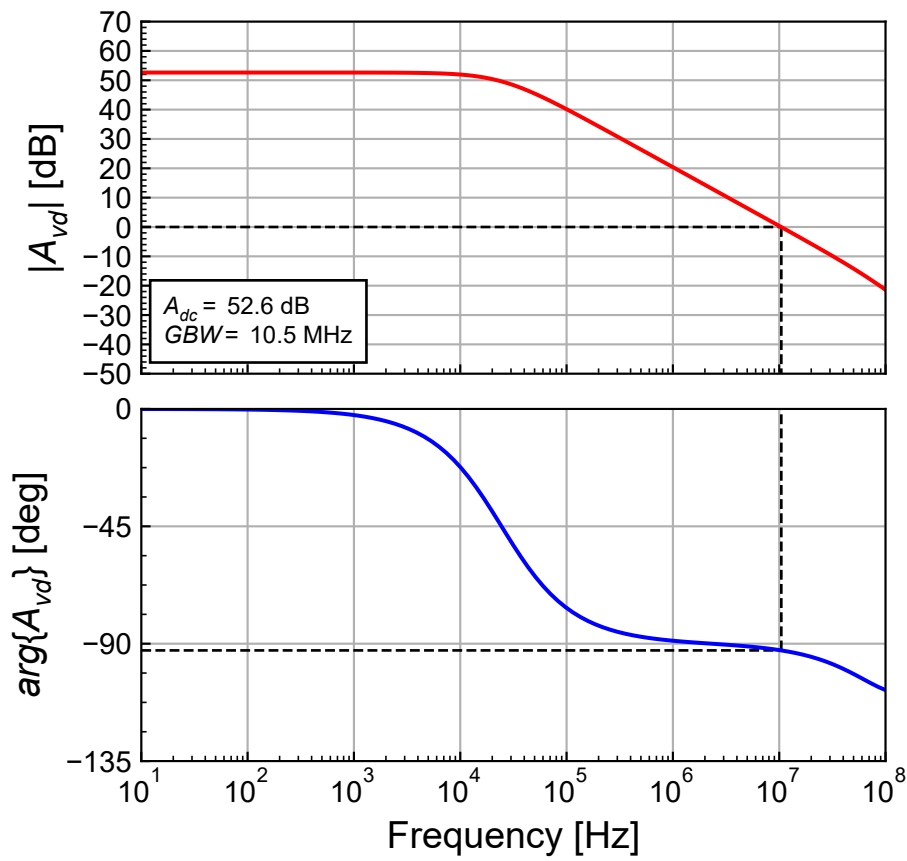


Figure 4.1: OTA theoretical transfer function.

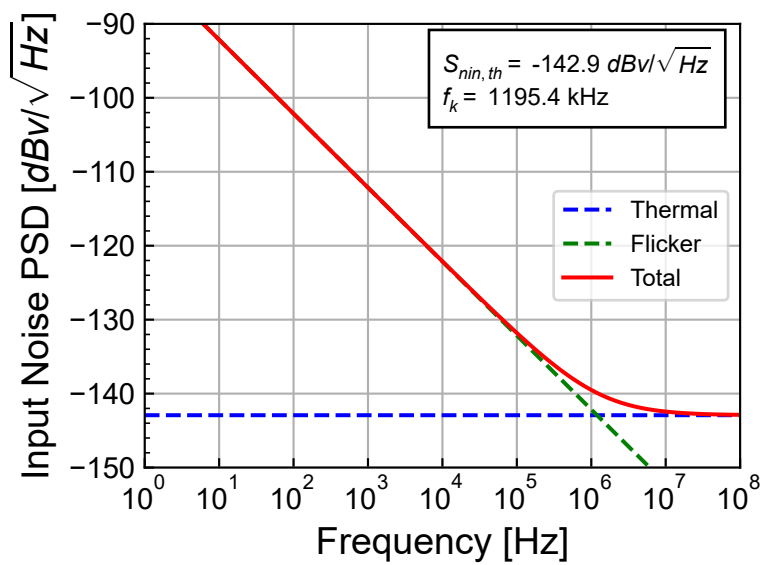


Figure 4.2: OTA theoretical input-referred noise PSD.

where

$$\sigma_{\beta_i}^2 = \frac{A_{\beta}^2}{W_i L_i} \quad i = 1, 2, \quad (4.6)$$

$$\sigma_{V_{T0i}}^2 = \frac{A_{VT}^2}{W_i L_i} \quad i = 1, 2. \quad (4.7)$$

The parameter for calculating the standard deviation of the input-referred offset voltage are given in Table 4.4.

Table 4.4: OTA input-referred offset parameters.

Symbol	Theoretical Value	Unit
σ_{VT1}	1.3444	<i>mV</i>
σ_{VT2}	9.28344	<i>mV</i>
$\sigma_{\beta1}$	0.268879	%
$\sigma_{\beta2}$	1.85669	%
ξ_{VT}	6.22439	-
ξ_{β}	47.6829	-
$\sigma_{V_T}^2$	13.0574	<i>mV</i> ²
σ_{V_T}	3.6135	<i>mV</i>
σ_{β}^2	0.998046	<i>mV</i> ²
σ_{β}	0.999022	<i>mV</i>
$\sigma_{V_{os}}$	3.749	<i>mV</i>

From Table 4.4, we see that the dominant contribution to the input-referred offset voltage is due to the differential pair M_{1a} - M_{1b} . The resulting total input-referred offset voltage is $\sigma_{V_{os}} = 3.749 \text{ mV}$.

4.4 Current and power consumption

The total current consumption without accounting for the bias string M_{3a} is simply $I_{tot} = 2 I_b = 700 \text{ nA}$, resulting in power consumption $P = V_{DD} \cdot I_{tot} = 1.3 \text{ }\mu\text{W}$.

5 Simulation results from ngspice

The theoretical results can be validated by comparing them to the results obtained from simulations performed with ngspice. The cells below will run the simulations with ngspice. In order to run the simulations you need to have ngspice installed. Please refer to the ngspice instructions.

i Note

The simulations are performed with ngspice [4] using the EKV 2.6 compact model [5] [12] [1]. For ngspice, we use the original Verilog-A implementation of EKV 2.6 [7] modified by C. Enz to get the operating point informations and available on the Gitub va-models site provided by D. Warning at [6] [13]. The Verilog-A code was then compiled with OpenVAF [14] to generate the OSDI for running it with ngspice. The parameters correspond to a generic 180 nm bulk CMOS process [8].

5.1 Operating point

We first write the parameter file for this specific design for running the ngspice simulations. Before running the AC and NOISE simulations, we first need to check the quiescent voltages and currents and the operating points of all transistors by running an .OP simulation. The node voltages are extracted from the .ic file and presented in Table 5.1.

Table 5.1: OTA node voltages with the OTA in open-loop without offset correction.

Node	Voltage
vdd	1.8
inp	0.9
inn	0.9
id	0
ic	0.9
out	1.087
1	0.419764
2	1.087
3	0.752329

From Table 5.1, we see that the output voltage $V_{outq} = 1087 \text{ mV}$ of the open-loop circuit is close to the input common mode voltage $V_{ic} = V_{DD}/2 = 900 \text{ mV}$. Since the operating point is in the high gain region, we don't need to impose an offset voltage to bring the output voltage in the high gain region.

The operating point information for all transistors coming from the EKV2.6 compact model are extracted from the ngspice .op.dat file. The data is split into the large-signal operating informations presented in Table 5.2, the small-signal operating point informations shown in Table 5.3 and the noise operating point informations in Table 5.4.

Table 5.2: Large-signal operating point information extracted from ngspice .op file for each transistor.

Transistor	I_D [nA]	I_{spec} [nA]	IC [-]	n [-]	V_{DSsat} [mV]
M1a	349.0	351.6	0.993	1.27	155
M1b	349.0	351.6	0.993	1.27	155
M2a	349.0	28.4	12.406	1.31	286
M2b	349.0	28.4	12.406	1.31	286
M3a	700.0	37.6	18.681	1.27	327
M3b	697.9	37.5	18.669	1.27	327

Table 5.3: Small-signal operating point information extracted from ngspice .op file for each transistor.

Transistor	G_m [$\mu A/V$]	G_{ms} [$\mu A/V$]	G_{ds} [nA/V]
M1a	6.455	8.313	2.566
M1b	6.455	8.313	2.566
M2a	2.456	3.308	5.544
M2b	2.456	3.308	5.544
M3a	4.222	5.441	4.881
M3b	4.208	5.427	8.822

Table 5.4: Noise operating point information extracted from ngspice .op file for each transistor.

Transistor	R_n [k Ω]	$\sqrt{S_{ID,th}}$ [nA/ \sqrt{Hz}]	γ_n [-]	$\sqrt{S_{ID,fl}}$ at 1Hz [nA/ \sqrt{Hz}]
M1a	114.185	43.506	0.737	8317.76
M1b	114.185	43.506	0.737	8317.76
M2a	350.763	76.251	0.861	150982
M2b	350.763	76.251	0.861	150982
M3a	200.120	57.595	0.845	31591.5
M3b	200.936	57.712	0.846	31591.5

We can check the bias voltages and operating region of each transistor which are given in Table 5.5.

Table 5.5: Bias voltages and operating regions of each transistor.

Trans.	Type	Funct.	V_G [V]	V_S [V]	V_D [V]	V_{DS} [mV]	V_{DSsat} [mV]	Reg.	Sat.
M1a	n	DP	0.480	0.000	0.667	667	155	MI	sat
M1b	n	DP	0.480	0.000	0.667	667	155	MI	sat
M2a	p	CM	0.713	0.000	0.713	713	286	SI	sat
M2b	p	CM	0.713	0.000	0.713	713	286	SI	sat
M3a	n	CM	0.752	0.000	0.752	752	327	SI	sat
M3b	n	CM	0.752	0.000	0.420	420	327	SI	sat

We see that all transistors are biased in saturation. The operating points looks fine. We can now proceed with the large-signal DC simulation.

5.2 Large-signal differential transfer characteristic

We now simulate the large-signal DC input-output transfer characteristic. The simulation result is presented in Figure 5.1.

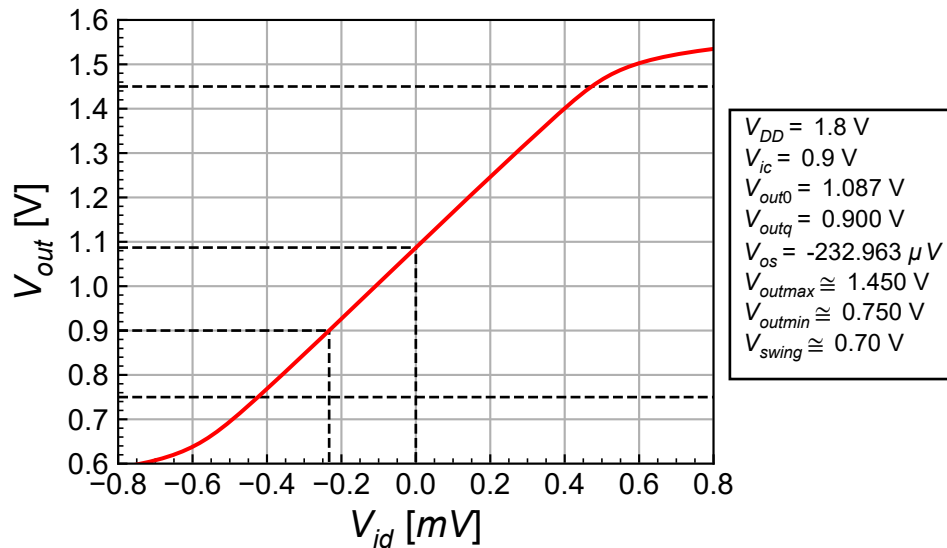


Figure 5.1: Simulated large-signal input-output characteristic.

From Figure 5.1, we see that the output swing is about $V_{out,swing} \cong 700 \text{ mV}$ which is rather small. We can now zoom into the high gain region and estimate the offset voltage and the output swing. The simulation results are presented in Figure 5.2.

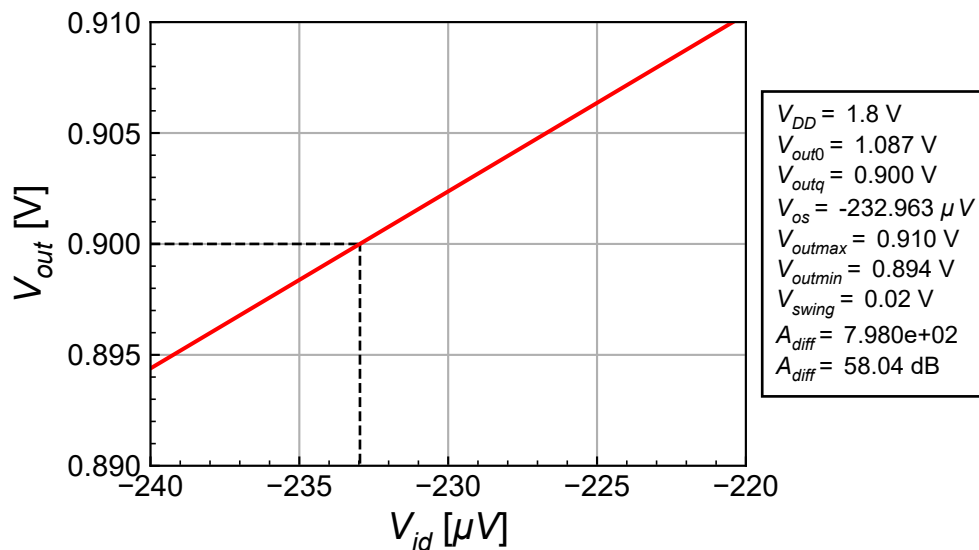


Figure 5.2: Zoom of the simulated large-signal input-output characteristic in the gain region.

We see that the required offset voltage to bring the output voltage to $V_{outq} = 900 \text{ mV}$ is equal to $V_{os} = -232.963 \text{ μV}$, which is small.

5.3 Open-loop gain

After having checked the operating point information and making sure that the OTA output is not saturated and in the high gain region, we can now perform the AC simulation. The simulation results are compared to the theoretical estimations in Figure 5.3.

We see an almost perfect match between the small-signal simulations and the theoretical results except at higher frequency where additional poles due to parasitic capacitances that have not been accounted

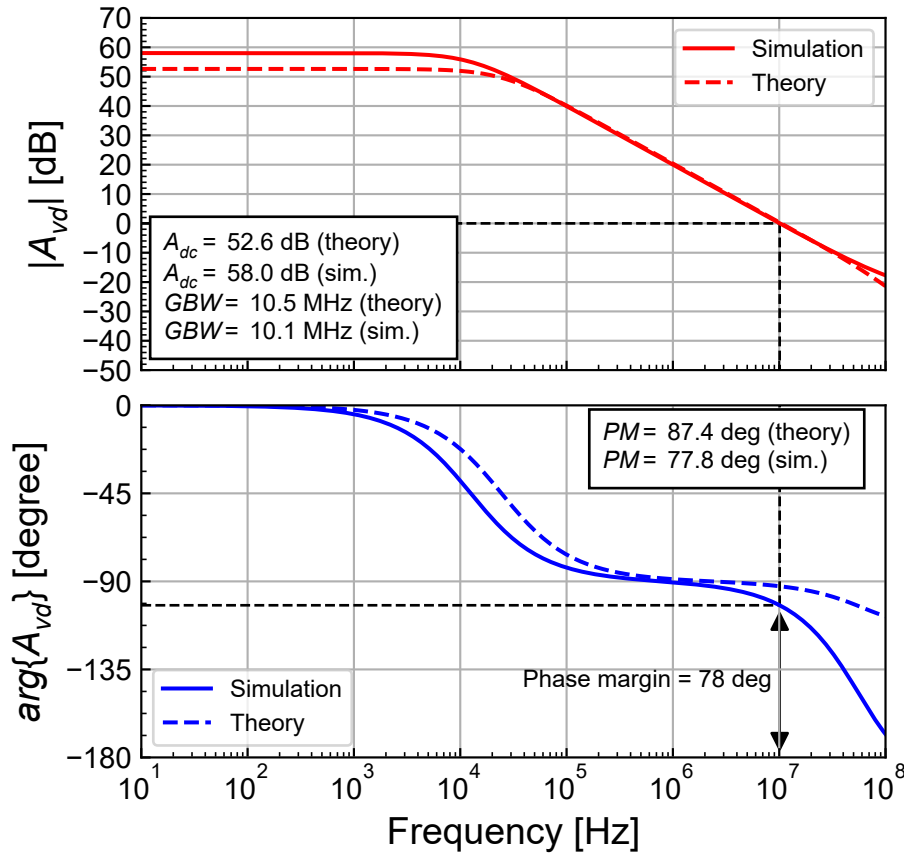


Figure 5.3: Simulated gain response compared to theoretical estimation.

for introduce additional phase shift. We now will perform the noise simulations.

5.4 Input-referred noise

We can compare the theoretical input-referred noise to that obtained from simulations. The simulation results are presented in Figure 5.4.

From Figure 5.4, we see a good match between the simulated and theoretical input-referred noise PSD. The contributions of M_{1a} - M_{1b} and M_{2a} - M_{2b} to the input-referred white noise PSD are detailed in Figure 5.5 and compared to the theoretical white noise.

We can observe that the total simulated white noise is about 0.306 dB higher than the theoretical estimation, which is acceptable. The white noise is dominated by the differential pair M_{1a} - M_{1b} which is $1 + \eta_{th} = 1.445$ times (or 1.599 dB) lower than the total white noise. The contribution of M_{2a} - M_{2b} is about $\eta_{th} = 0.445$ times (or 3.516 dB) lower than the contribution of M_{1a} - M_{1b} . The simulated value of $\eta_{th} = 0.445$ is about 1.075 larger than the theoretical estimation. This results in an OTA thermal noise excess factor $\gamma_{n,ota} = 2.135$ that is slightly larger than the predicted value $\gamma_{n,ota} = 2.026$.

Figure 5.6 presents the breakdown of the contributions of M_{1a} - M_{1b} and M_{2a} - M_{2b} to the input-referred flicker noise. Contrary to the white noise, the flicker noise is largely dominated by the contribution of the current mirror M_{2a} - M_{2b} which was already observed in the OTA characteristic section. It is due to the fact that $W_1 L_1$ is 48 times larger than $W_2 L_2$ and that ρ_p is 8.3 times larger than ρ_n .

The breakdown of the contributions of M_{1a} - M_{1b} and M_{2a} - M_{2b} to the total input-referred noise is summarized in Figure 5.6. We can observe that the simulation is close to the theoretical estimation.

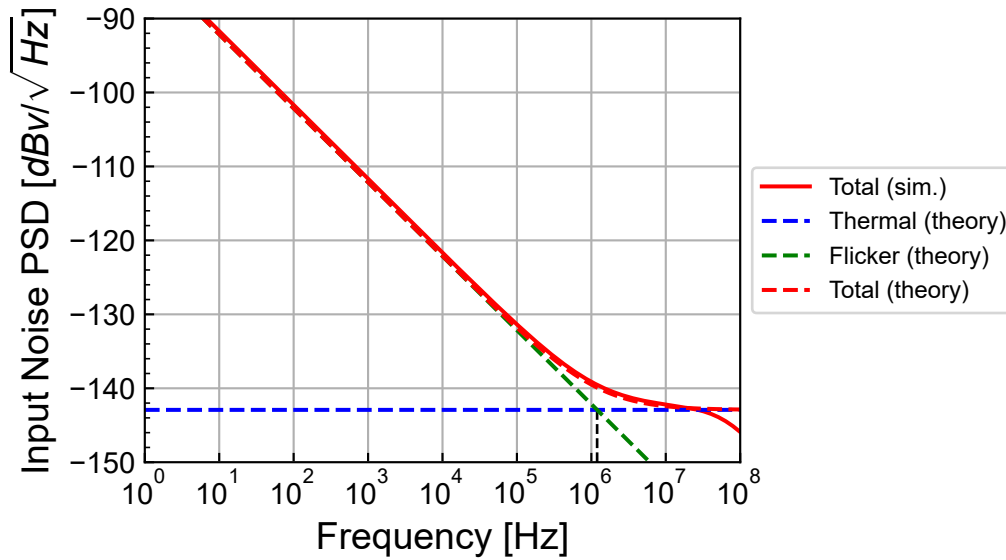


Figure 5.4: Simulated input-referred noise PSD compared to theoretical estimation.

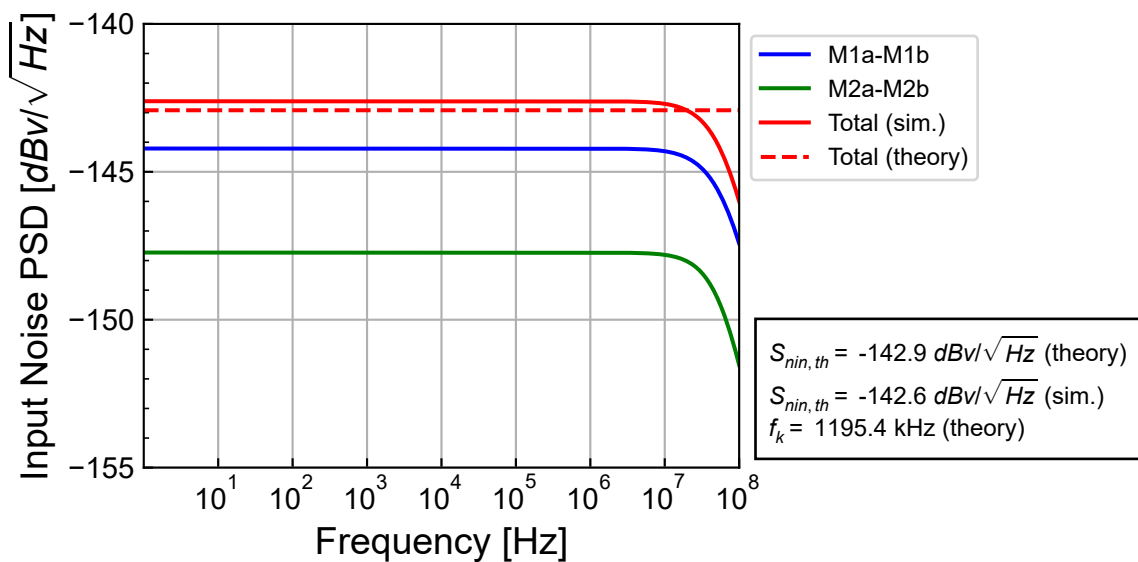


Figure 5.5: Breakdown of the contributions to the simulated input-referred white noise PSD.

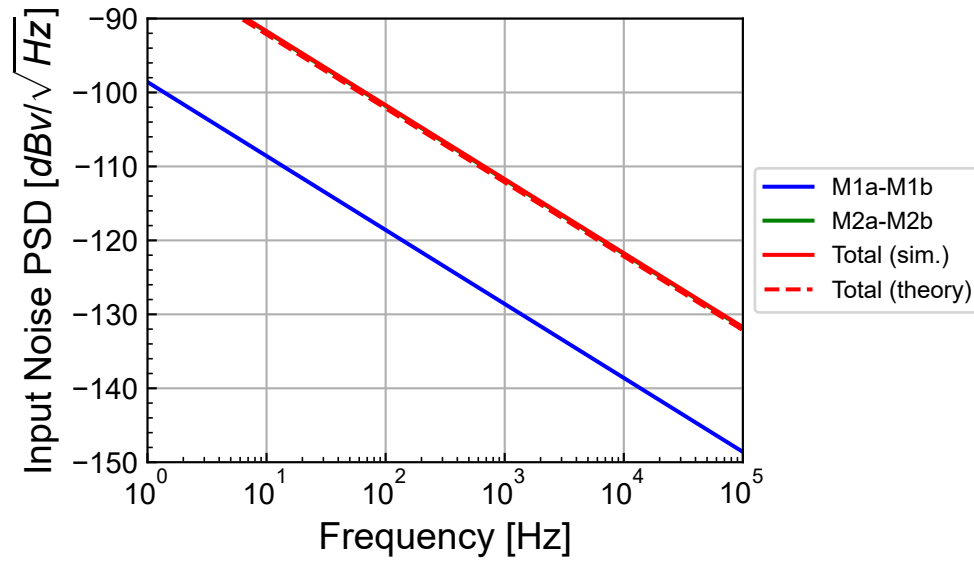


Figure 5.6: Breakdown of the contributions to the simulated input-referred flicker noise PSD.

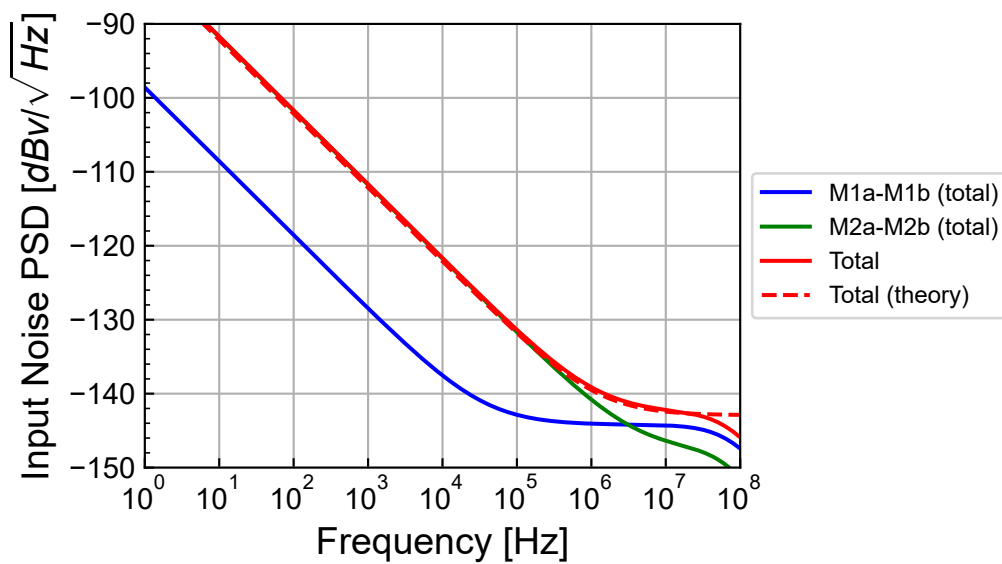


Figure 5.7: Breakdown of the contributions to the simulated input-referred noise PSD.

5.5 Input common-mode voltage range

We can check the input common-mode voltage range by connecting the OTA as a voltage follower and sweeping the positive input. The result is shown in Figure 5.8.

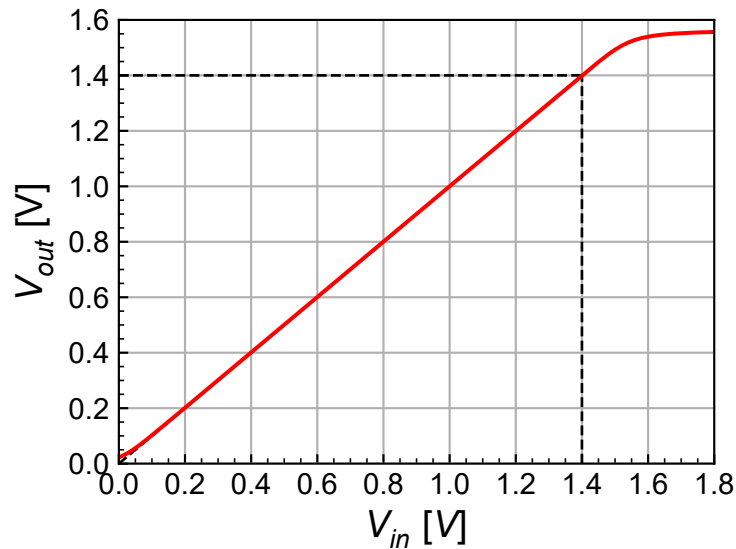


Figure 5.8: Simulated input common-mode voltage range.

As shown in Figure 5.8, the output follows the input voltage up to 1.4 V. So the input common-mode voltage range is about 1.4 V.

5.6 Step-response

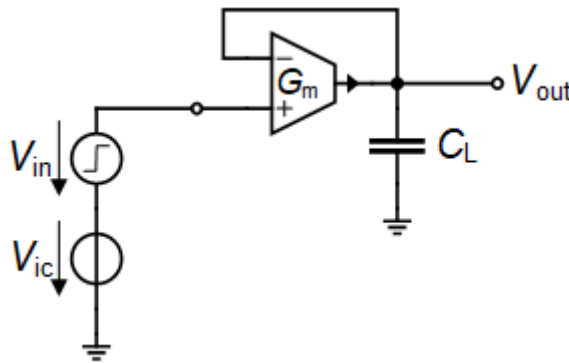


Figure 5.9: Schematic of the OTA connected as a voltage follower.

In this section we will check the step response of the OTA operating as a voltage follower as shown in Figure 5.9 with its output connected to the negative input and with the same load capacitance $C_L = 0.1 \text{ pF}$. According to the input common-mode voltage range established above, we will set the input common-mode voltage to $V_{ic} = 0.9 \text{ V}$ to leave enough room for the large step.

5.6.1 Small-step

We start by imposing a small step $\Delta V_{in} = 10 \text{ mV}$ on top of a common mode voltage $V_{ic} = 0.9 \text{ V}$. The simulation results are shown in Figure 5.10 where $\Delta V_{in}(t) \triangleq V_{in+}(t) - V_{ic}$ and $\Delta V_{out}(t) \triangleq V_{out}(t) - V_{outq}$ with V_{outq} the quiescent output voltage at the operating point before the step is applied. ΔV_{in} and

ΔV_{out} are compared to the response of a single pole circuit having a cut-off frequency equal to the GBW . We can observe a very good match between the simulated and theoretical small step response.

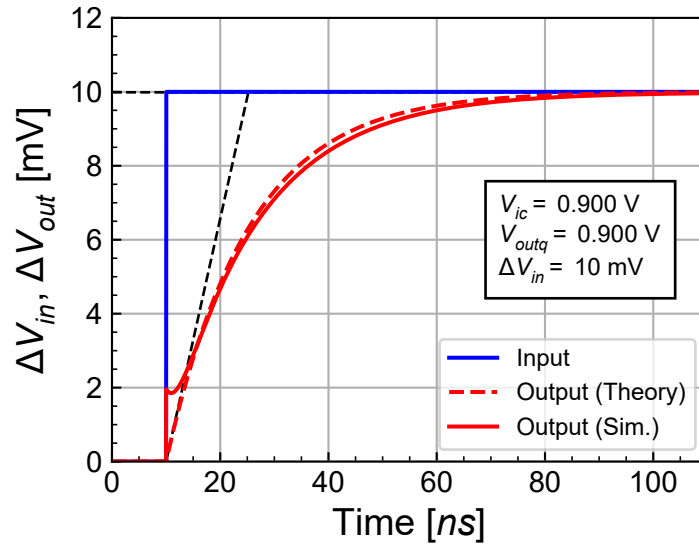


Figure 5.10: Step response of the OTA as a voltage follower for a small input step.

5.6.2 Large step

We now impose a larger step $\Delta V_{in} = 300$ mV on top of a common mode voltage $V_{ic} = 300$ mV. The simulation results are shown in Figure 5.11 where $\Delta V_{in}(t) \triangleq V_{in+}(t) - V_{ic}$ and $\Delta V_{out}(t) \triangleq V_{out}(t) - V_{outq}$ with V_{outq} the quiescent output voltage at the operating point before the step is applied. ΔV_{in} and ΔV_{out} are compared to the response of a single pole circuit having a cut-off frequency equal to the GBW . We now observe the effect of slew-rate which increases the settling time.

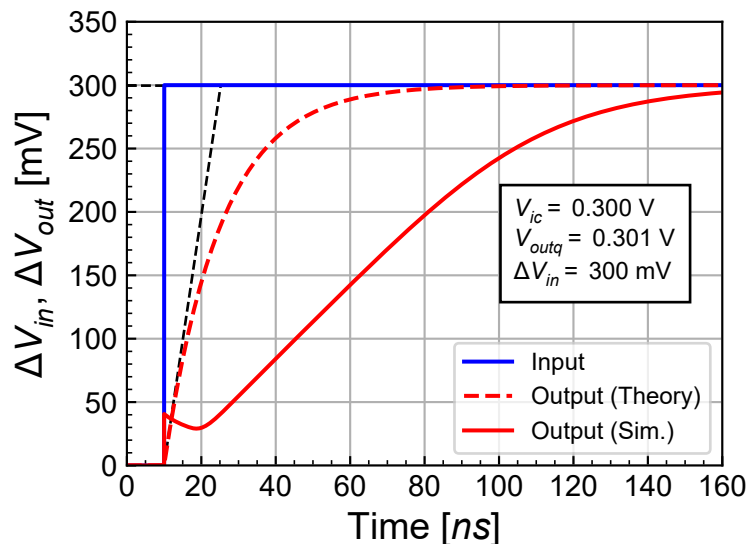


Figure 5.11: Step response of the OTA as a voltage follower for a large input step highlighting the slew-rate effect.

5.7 Current and power consumption

The total current consumption without accounting for the bias string M_{3a} is simply $I_{tot} = 2 I_b = 700$ nA, resulting in power consumption $P = V_{DD} \cdot I_{tot} = 1.3 \mu W$.

6 Conclusion

This notebook presented the analysis, design and verification of the simple 5 transistors OTA. The detailed analysis provided all the equations that were then used in the design phase to reach the target specifications. The design was then performed using the inversion coefficient approach with the sEKV transistor model for a generic 180 nm bulk CMOS process. The theoretical performance resulting from the design were then evaluated. The design was then verified by simulation with ngspice [4] using the EKV 2.6 compact model [5] [12] [1] and the parameters of a generic 180 nm bulk CMOS process. After carefully checking the operating point, the large-signal transfer characteristic was simulated. Then the small-signal open-loop transfer function was simulated. The target gain-bandwidth GBW and DC gain are achieved. The input-referred noise was then simulated and compared to the theoretical estimation. It was shown that the flicker noise is dominated by the pMOS current mirror, while the white noise is dominated by the differential pair. The input common-mode voltage range was then simulated with the OTA connected as a voltage follower. The input voltage is limited to 1.4 V. Finally, the small-signal step response was simulated and successfully compared to the theoretical small step response. The step-response with a large input step highlighted the effect of slew-rate resulting in an increased settling time.

References

- [1] C. C. Enz and E. A. Vittoz, *Charge-Based MOS Transistor Modeling - The EKV Model for Low-Power and RF IC Design*, 1st ed. John Wiley, 2006.
- [2] C. Enz, F. Chicco, and A. Pezzotta, “Nanoscale MOSFET Modeling: Part 1: The Simplified EKV Model for the Design of Low-Power Analog Circuits,” *IEEE Solid-State Circuits Magazine*, vol. 9, no. 3, pp. 26–35, 2017.
- [3] C. Enz, F. Chicco, and A. Pezzotta, “Nanoscale MOSFET Modeling: Part 2: Using the Inversion Coefficient as the Primary Design Parameter,” *IEEE Solid-State Circuits Magazine*, vol. 9, no. 4, pp. 73–81, 2017.
- [4] Holger Vogt, Giles Atkinson, Paolo Nenzi, “Ngspice User’s Manual Version 43.” <https://ngspice.sourceforge.io/docs/ngspice-43-manual.pdf>, 2024.
- [5] M. Bucher, C. Lallement, C. Enz, F. Théodoloz, and F. Krummenacher, “The EPFL-EKV MOSFET Model Equations for Simulation.” https://github.com/chrisenz/EKV/blob/main/EKV2.6/docs/ekv_v26_rev2.pdf, 1998.
- [6] M. Bucher, C. Lallement, C. Enz, F. Théodoloz, and F. Krummenacher, “EKV 2.6 Verilog-A Code.” <https://github.com/chrisenz/EKV/tree/main/EKV2.6/va/code>, 2024.
- [7] W. Grabinski *et al.*, “FOSS EKV2.6 verilog-a compact MOSFET model,” in *European solid-state device research conference (ESSDERC)*, 2019, pp. 190–193. doi: [10.1109/ESSDERC.2019.8901822](https://doi.org/10.1109/ESSDERC.2019.8901822).
- [8] W. Grabinski *et al.*, “FOSS EKV 2.6 parameter extractor,” in *2015 22nd international conference mixed design of integrated circuits & systems (MIXDES)*, 2015, pp. 181–186. doi: [10.1109/MIXDES.2015.7208507](https://doi.org/10.1109/MIXDES.2015.7208507).
- [9] Han, H.-C. and A. D’Amico and C. Enz, “SEKV-E: Parameter Extractor of Simplified EKV I-V model for Low-power Analog Circuits.” <https://gitlab.com/moscm/sekv-e>, 2022.
- [10] F. Krummenacher, E. Vittoz, and M. Degrauwe, “Class AB CMOS amplifier micropower SC filters,” *Electronics Letters*, vol. 17, no. 13, pp. 433–435, 1981.
- [11] M. G. Degrauwe, J. Rijmenants, E. A. Vittoz, and H. J. D. Man, “Adaptive biasing CMOS amplifiers,” *IEEE Journal of Solid-State Circuits*, vol. 17, no. 3, pp. 522–528, 1982.
- [12] C. C. Enz, F. Krummenacher, and E. A. Vittoz, “An Analytical MOS Transistor Model Valid in All Regions of Operation and Dedicated to Low-Voltage and Low-Current Applications,” *Analog Integrated Circuits and Signal Processing Journal*, vol. 8. https://github.com/chrisenz/EKV/tree/main/EKV2.6/docs/EKV_original_paper_1995_prepub.pdf, pp. 83–114, 1995.
- [13] Dietmar Warning, “Verilog-A Models for Circuit Simulation.” <https://github.com/dwarning/VA-Models>, 2024.
- [14] SemiMod GmbH, “Open VAF.” <https://openvaf.semimod.de/docs/getting-started/introduction/>, 2025.